J. Mech. Phys. Solids 168 (2022) 105052

Contents lists available at ScienceDirect

Journal of the Mechanics and Physics of Solids

journal homepage: www.elsevier.com/locate/jmps

Delayed tensile instabilities of hydrogels

Jie Ma [a], Daochen Yin [a], Zhi Sheng [a], Jian Cheng [b], Zheng Jia [a,*], Teng Li [b], Shaoxing Qu [a]

[a] Key Laboratory of Soft Machines and Smart Devices of Zhejiang Province, Center for X-Mechanics, Department of Engineering Mechanics, Zhejiang University, Hangzhou 310027, People's Republic of China
[b] Department of Mechanical Engineering, University of Maryland, College Park, Maryland 20742, USA

ARTICLE INFO

Keywords:
Instability
Necking
Burst
Bulging
Hydrogels

ABSTRACT

Soft materials can undergo various deformation instabilities, including wrinkling, creasing, and necking. Most existing studies of such instabilities of soft materials consider instant instability, which occurs instantaneously when the applied load exceeds a threshold level. Herein, we uncover the delayed tensile instability of hydrogels, a largely unstudied instability mode for soft materials. As the name suggests, when subject to a certain level of tensile load, a hydrogel may remain stable initially, and then suddenly become unstable after a delay in time. We find the delayed instability mode of hydrogels of various shapes, including the necking of stretched double-network hydrogel bars, the burst of pressurized spherical balloons, and the bulging of inflated cylindrical tubes. We reveal that tension-induced water absorption of hydrogels is the key mechanism underpinning the delayed tensile instabilities. The results from this study shed light on new guidelines in designing hydrogels to mitigate or harness deformation instabilities.

1. Introduction

The instability of soft materials and structures has long been a focal topic of the mechanics and physics of solids. A variety of instabilities – such as wrinkling (Huang, 2005; Li et al., 2011), ridging (Zang et al., 2012), buckling (Chen and Jin, 2020; Jawed et al., 2015; Mullin et al., 2007; Rafsanjani and Bertoldi, 2017; Yin et al., 2008), creasing (Cai et al., 2012; Chen et al., 2012; Jin and Suo, 2015; Liu et al., 2019), cratering (Wang et al., 2011), cavitation (Fu et al., 2020), and Rayleigh-Taylor instability (Zheng et al., 2019) – can be triggered when soft bodies are subjected to mechanical loadings or electric fields. While most instabilities arise under compressive forces, structures and materials may also become unstable under tensile stresses – the phenomenon is widely referred to as tensile instability. For example, when inflating a rubber balloon, the wall of the balloon is stretched by the internal-pressure-induced biaxial tensile stresses. Once the internal pressure reaches a critical value, the balloon expands in volume suddenly and unboundedly, often leading to the burst of the balloon (Cheng et al., 2019; Overvelde et al., 2015). Similarly, in an inflated cylindrical rubber tube subjected to internal pressure, localized bulging of one section of the tube can occur as a critical pressure level is approached (Fu et al., 2016; Ye et al., 2020). Similar instability in a blood vessel attributes to the formation of aneurysm (Bogen and McMahon, 1979). In addition, Na et al. experimentally observe the initiation and propagation of necking instability in double-network hydrogels (DN gels) during uniaxial-tension tests (Na et al., 2006).

Notably, most above-mentioned research on instabilities assumes a closed system in thermodynamics, such as hyperelastic rubbers

* Corresponding author.
E-mail address: zheng.jia@zju.edu.cn (Z. Jia).

https://doi.org/10.1016/j.jmps.2022.105052
Received 5 March 2022; Received in revised form 10 July 2022; Accepted 29 August 2022
Available online 30 August 2022

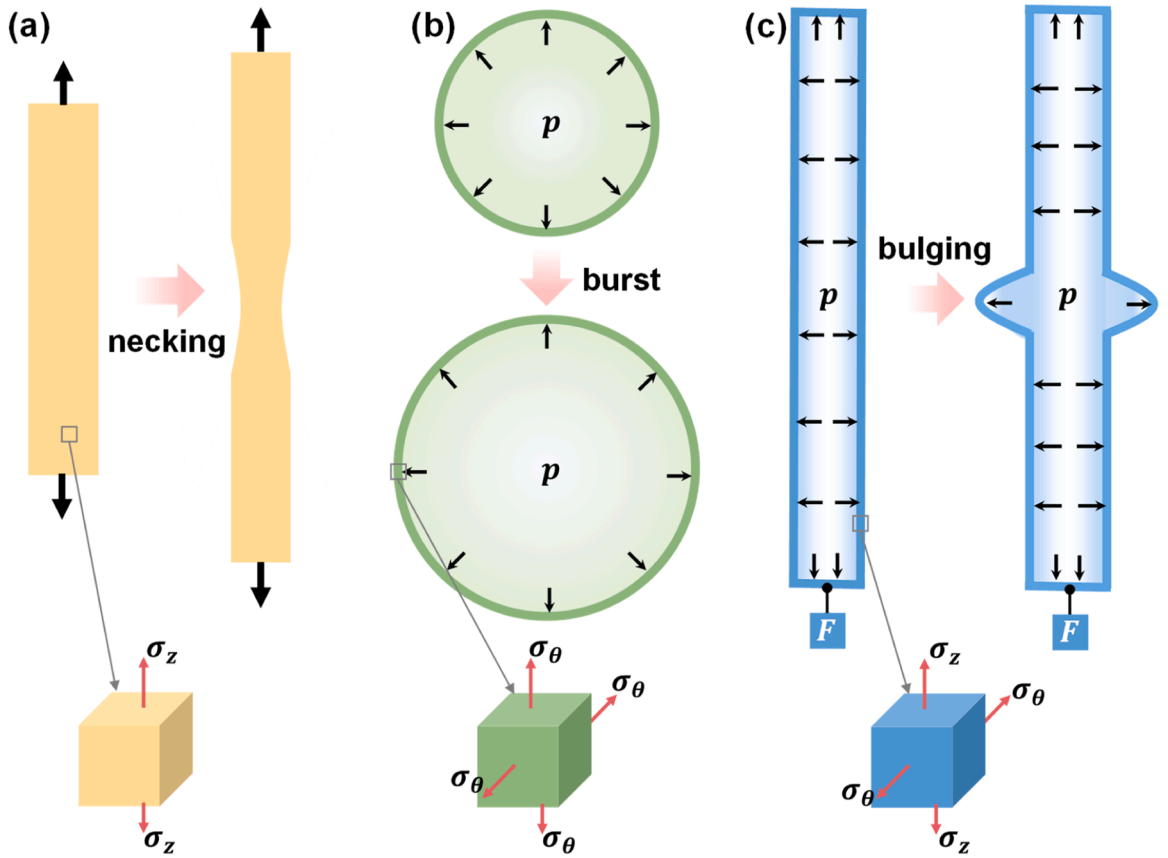

Fig. 1. Schematics of three representative delayed tensile instabilities of hydrogel structures. (a) Delayed necking of a stretched double-network hydrogel bar. The hydrogel is under uniaxial tension. (b) Delayed burst of an inflated spherical hydrogel balloon. The wall of the balloon is subjected to equi-biaxial tension induced by the internal pressure p. (c) Delayed bulging of a pressurized cylindrical tube. The wall of the tube is stretched by biaxial tension. p and F represent the internal pressure and the weight hanging at the end of the tube, respectively.

or hydrogels that deform over a short time scale, so that the materials do not exchange any matter with their surroundings. Recently, hydrogels have been employed in diverse applications, including medical implants (Yang et al., 2021), drug delivery (Li and Mooney, 2016), tissue engineering (Yuk et al., 2019), and stimuli-sensitive actuators (Han et al., 2020). For these applications, the assumption of closed systems in thermodynamics is no longer valid: hydrogels are constantly in contact with water and subject to mechanical loads for an extended duration of time, allowing the transport of water molecules in and out of the gel. Such mass transport is intrinsically coupled with the deformation of the hydrogels and can significantly affect the mechanical response of hydrogels. For instance, Tang et al. reveal that, when a chemically crosslinked hydrogel containing a pre-cut crack is stretched and held at a constant strain level, the crack remains stationary in the beginning and then suddenly grows significantly after a time of delay (Tang et al., 2017). This phenomenon has been termed the delayed fracture by Wang and Hong, which is attributed to the diffusion and redistribution of water molecules driven by the crack-tip stress field (Wang and Hong, 2012). Since fracture and instability are both triggered by critical mechanical loads exceeding a threshold, a natural question to ask is whether new instability modes exist in open-system hydrogels – which are under mechanical loads and can exchange water molecules with the surroundings.

In this study, we uncover a new instability mode of hydrogels – the delayed tensile instability. We use the necking formation of DN gels as an example to illustrate the concept of delayed tensile instability [Fig. 1(a)]. Under a monotonic load that rapidly increases at a constant rate, the hydrogel elongates uniformly in the beginning, and then necking suddenly forms when the load reaches a critical level. Such instability under a monotonic load is called *instant instability* and the load at which instant instability occurs is called the threshold for instant instability. The aforementioned necking instability of DN gels (Na et al., 2006), as well as the burst of pressurized rubber balloons and the bulging of inflated soft tubes (Fu et al., 2016; Overvelde et al., 2015), all fall into the category of instant instability. Under static load, where a load is rapidly applied and then held at a constant level slightly lower than the threshold for instant instability, the hydrogel remains stable for a span of time, and then develops necking instability suddenly after a delay in time. When the static load is at a level way below the threshold for instant instability, the DN gel remains stable all the time, not susceptible to either instant or delayed instability. We define the instability under static load as *delayed instability*, and call the load above which delayed instability occurs the threshold for delayed instability. We further demonstrate that tensile stress state is a necessary condition for triggering delayed necking of DN gels, thus delayed instability of hydrogels should be called delayed tensile instability in a precise

manner. In addition, delayed tensile instability also occurs in pressurized hydrogel balloons [Fig. 1(b)] and inflated cylindrical hydrogel tubes [Fig. 1(c)] that are in contact with water. We expect that most tensile instabilities of hydrogels have a delayed instability mode.

The rest of this paper is organized as follows. In section 2, we derive the free energy function of the DN gel, taking the change of water concentration inside the gel into consideration. Three instability/deformation modes are demonstrated for DN gels under uniaxial tension, including instant necking, delayed necking, and equilibrium swelling without necking. In Section 3, we reveal that an inflated spherical hydrogel balloon, the wall of which is under equi-biaxial tension, may also be subject to delayed tensile instability – the delayed burst caused by postponed snap-through instability of the balloon. In Section 4, we further reveal that delayed tensile instability – delayed bulging – may occur in a pressurized cylindrical tube, the wall of which is biaxially stretched. In Section 5, the universality of the delayed tensile instability is discussed. Section 6 summarizes the main findings of the paper.

2. Delayed necking of stretched double-network hydrogels

2.1. Deformation, swelling, and damage of DN gels

A DN gel is an aggregate of water molecules and two interpenetrating polymer networks with distinct chain lengths – a long-chain network (network L) and a short-chain network (network S) (Na et al., 2006). The two networks are interlaced on a molecular scale but not covalently bonded to each other (Zhao, 2012). The necking instability of DN gels is a consequence of the deformation-induced stiffening of the long-chain network and the damage-induced softening of the short-chain network.

When considering the deformation of the two polymer networks, we assume polymer chains of one network are stretched isotropically and homogeneously by the interpenetration of the other network (Zhao, 2012), and take the dry polymer networks as the reference state (Hong et al., 2009; Hong et al., 2008). Let Λ_i ($i = S,\ L$) be the stretch of each chain of the network i ($i = S$ represents the short-chain network and $i = L$ represents the long-chain network), we have $\Lambda_i = \eta_i^{-\frac{1}{3}}\sqrt{(\lambda_1^2+\lambda_2^2+\lambda_3^2)/3}$, where λ_1, λ_2, and λ_3 are the stretches of the DN gel relative to the reference state, and η_i the volume fraction of the network i in the dry polymer networks. Moreover, the volume of the gel is the sum of the volume of the dry networks and the volume of the water phase. Under mechanical loads, the long polymer chains and small water molecules can undergo large configurational change without appreciable volumetric change. Following common practice, we assume that all individual molecules in the gel are incompressible, so that $\lambda_1\lambda_2\lambda_3 = 1 + \nu C$, where ν is the volume per water molecule and C is the water concentration defined as the number of water molecules per volume of the dry network.

In thermodynamics, the deformation of the DN gel under mechanical loads is governed by its free energy function, which comes from two molecular processes – (1) stretching polymer chains in the polymer networks, and (2) mixing polymer networks and water molecules. Following Flory and Rehner (Flory and Rehner, 1943), the free energy function of the DN gel per reference volume takes the form

$$W = \sum_{i=L,\ S} W_i^s + W^m, \tag{1}$$

where W_i^s is the free energy due to stretching the network i per reference volume, and W^m is the free energy due to mixing polymer networks and solvents per reference volume. The free energy due to stretching W_i^s can be calculated as

$$W_i^s = \eta_i N_i n_i kT\left(\frac{\beta_i}{tanh\beta_i} + \log\frac{\beta_i}{sinh\beta_i}\right), \tag{2}$$

where kT is the temperature in the unit of energy, N_i the number of chains of the network i per unit volume of the network i, n_i the number of freely jointed links on a chain of the network i. The chain force β_i relates to the stretch Λ_i as $\Lambda_i = \sqrt{n_i}\left(\frac{1}{\tanh\beta_i} - \frac{1}{\beta_i}\right)$ (Treloar and Riding, 1979). The free energy of mixing W^m depends on the water content in the DN gel and takes the form that (See details of the derivation in Appendix A)

$$W^m = \frac{kT}{\nu}\left[(J-1)log\frac{J-1}{J} + \sum_{i=L,\ S}\eta_i\chi_i\frac{J-1}{J}\right], \tag{3}$$

where χ_i is a dimensionless measure of the strength of pairwise interactions between water molecules and monomers of the network i. $J = \lambda_1\lambda_2\lambda_3 = 1 + \nu C$ is the swelling ratio of the gel defined with respect to the dry polymer networks and measures the water content in the DN gel. In the absence of mechanical load and geometrical constraint, the DN gel swells and equilibrates with water in its surroundings with isotropic stretches: $\lambda_1 = \lambda_2 = \lambda_3 = \lambda_0$, with the initial swelling ratio of the gel being $J_0 = \lambda_0^3$.

The damage of DN gels under deformation is attributed to the breaking of polymer chains in the short-chain network. As the short-chain network is stretched, the chains in the network break sequentially. As a result, some of the chains become inactive terminal chains, reducing the chain density of the short-chain network, while other chains rearrange into longer chains, giving rise to increasing numbers of links on a chain of the short-chain network (Zhao, 2012). Let N_{S0} and n_{S0} be chain density and number of links per chain in the pristine short-chain network before deformation, such that the physical picture above can be captured by

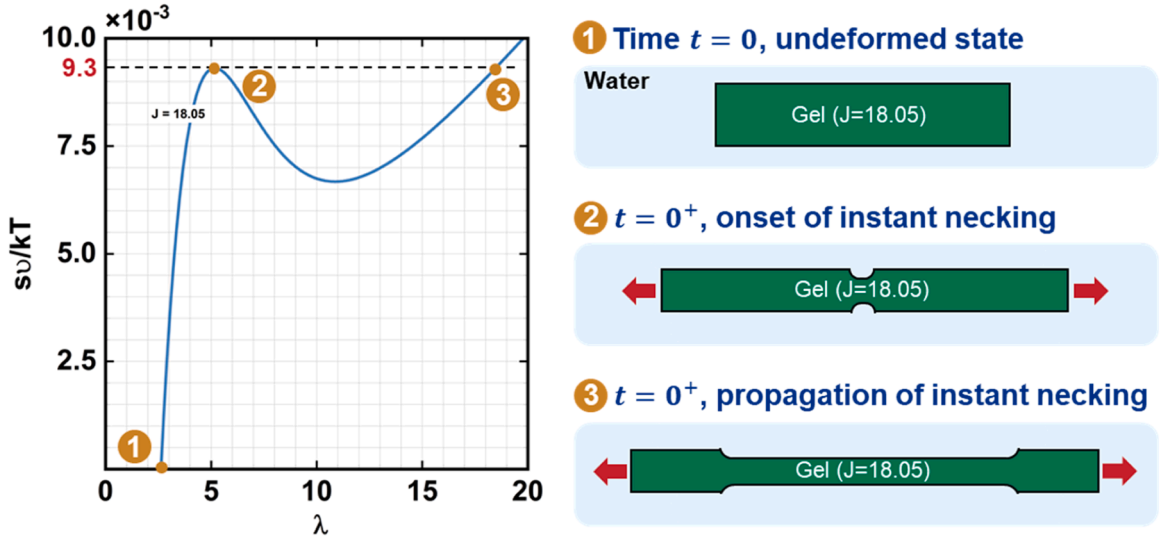

Fig. 2. Instant necking instability of DN gels under uniaxial tension. The mechanism for the instant necking instability can be illustrated by the instantaneous stress-stretch curve of a DN gel subject to uniaxial tension. When a uniaxial tensile force is rapidly applied to the DN gel sample, the original gel (point 1) elongates uniformly in the beginning, and then necking instability occurs instantaneously when the applied load reaches a critical level – the peak value of the curve (point 2). Note that the uniaxial tensile force is rapidly applied to the DN gel so that the short time interval (from time $t = 0$ to $t = 0^+$) before necking initiation does not allow the change of water content.

$N_S = N_{S0}\exp[-p(\Lambda_S^{max} - \eta_S^{-1/3})]$ and $n_S = n_{S0}\exp[q(\Lambda_S^{max} - \eta_S^{-1/3})]$. Here p and q are material parameters to characterize the decrease of chain density and increase of chain length. $\Lambda_S^{max} = \underset{0\le\tau\le t}{max}[\Lambda_S(\tau)]$ is the maximum stretch experienced by the chains of the short-chain network until the current time t.

In the following, we use representative values $p = q = 0.3698$ (Zhao, 2012), $\eta_S = 0.1$ (Zhao, 2012), $\eta_L = 0.9$ (Zhao, 2012), $n_{S0} = 50$ (Zhao, 2012), $n_L = 2000$ (Zhao, 2012), $\chi_L = \chi_S = 0.1$ (Hong et al., 2009), which specify a DN gel with free-swelling swelling ratio of $J_0 = 18.05$ (Details about the calculation of J_0 can be found in Appendix B). We will take this DN gel as the example to explicate the mechanism underpinning the delayed necking instability of DN gels.

2.2. *Instant necking instability of DN gels*

The migration of water in and out of the gel takes time. As a result, when a uniaxial tensile force is rapidly applied to the DN gel sample, the short time interval does not allow redistribution of water, and thus the water concentration C in the gel remains unchanged during stretching in such a short time. That is, the instantaneous deformation of the DN gel is volume-conserving with the swelling ratio being a constant ($J = \lambda_1\lambda_2\lambda_3 = \widehat{J} = const$). To impose the incompressibility condition, we introduce a Lagrange multiplier Π to the free energy function W, which yields

$$\widehat{W} = W + \Pi(J - \widehat{J}), \tag{4}$$

where $W = \sum_{i=L,\ S} W_i^s + W^m$. Note that for the instantaneous stress-stretch response, J is fixed. Therefore, according to Eq. (3), the free energy of mixing W^m becomes a constant and does not contribute to the mechanical stresses. In this regard, taking the derivative of $\widehat{W}$ with respect to principal stretches, we have the nominal stresses in principal directions as

$$s_1 = \frac{\partial\widehat{W}}{\partial\lambda_1} = \frac{\partial\sum_{i=L,\ S} W_i^s}{\lambda_1} + \Pi\lambda_2\lambda_3 = \left(\frac{\eta_S^{\frac{1}{3}} N_S\sqrt{n_S}kT\beta_S}{3\Lambda_S} + \frac{\eta_L^{\frac{1}{3}} N_L\sqrt{n_L}kT\beta_L}{3\Lambda_L}\right)\lambda_1 + \Pi\lambda_2\lambda_3, \tag{5a}$$

$$s_2 = \frac{\partial\widehat{W}}{\partial\lambda_2} = \frac{\partial\sum_{i=L,\ S} W_i^s}{\lambda_1} + \Pi\lambda_1\lambda_3 = \left(\frac{\eta_S^{\frac{1}{3}} N_S\sqrt{n_S}kT\beta_S}{3\Lambda_S} + \frac{\eta_L^{\frac{1}{3}} N_L\sqrt{n_L}kT\beta_L}{3\Lambda_L}\right)\lambda_2 + \Pi\lambda_1\lambda_3, \tag{5b}$$

$$s_3 = \frac{\partial\widehat{W}}{\partial\lambda_3} = \frac{\partial\sum_{i=L,\ S} W_i^s}{\lambda_3} + \Pi\lambda_1\lambda_2 = \left(\frac{\eta_S^{\frac{1}{3}} N_S\sqrt{n_S}kT\beta_S}{3\Lambda_S} + \frac{\eta_L^{\frac{1}{3}} N_L\sqrt{n_L}kT\beta_L}{3\Lambda_L}\right)\lambda_3 + \Pi\lambda_1\lambda_2. \tag{5c}$$

When the DN gel is subjected to uniaxial tension, we have $s_1 = s$ and $s_2 = s_3 = 0$; the stretches are $\lambda_1 = \lambda$ and $\lambda_2 = \lambda_3 = \sqrt{J/\lambda}$. The Lagrange multiplier Π can be solved by setting $s_2 = 0$ in Eq. (5b)

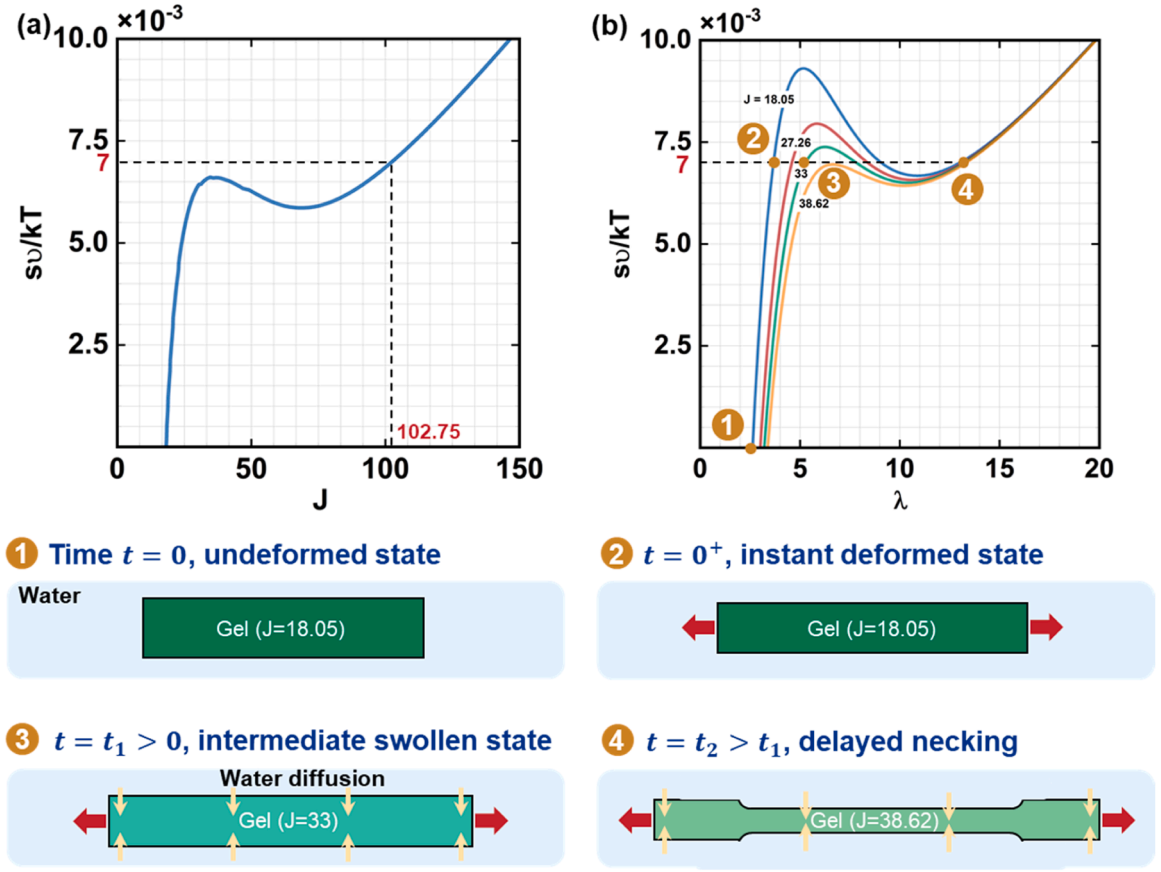

Fig. 3. *Delayed necking instability of DN gels under uniaxial tension. (a) The long-term equilibrium deformation of the DN gel under uniaxial tension. Under tensile stress, DN Gels gradually absorb water and swell. For example, when subjected to a static stress of* $\frac{s\nu}{kT} = 7 \times 10^{-3}$*, the DN gel can swell from its initial swelling ratio of* $J = 18.05$ *to* 102.75*. (b) The instantaneous stress-stretch curves of DN gels with different water contents. The peak value of the stress-stretch curve drops as the swelling ratio J increases. The delayed necking instability occurs if the peak value decreases to the applied stress level. The static stress* $\frac{s\nu}{kT} = 7 \times 10^{-3}$ *triggers the necking instability when the DN gel swells to* $J = 38.62$*. The swelling process of gels takes time, which accounts for the delay in necking formation (the load is applied at time* $t = 0$*, while the necking occurs at* $t = t_2 > 0$*). In all schematics, the change in color of the gel from dark green to light green indicates a gradual increase in the water content of the hydrogel.*

$$\Pi = -\left(\frac{\eta_S^{\frac{1}{3}} N_S \sqrt{n_S} kT\beta_S}{3\Lambda_S} + \frac{\eta_L^{\frac{1}{3}} N_L \sqrt{n_L} kT\beta_L}{3\Lambda_L}\right) \frac{1}{\lambda}. \tag{6}$$

Insert Eq. (6) into Eq. (5a), we obtain the nominal stress as

$$s = \left(\frac{\eta_S^{\frac{1}{3}} N_S \sqrt{n_S} kT\beta_S}{3\Lambda_S} + \frac{\eta_L^{\frac{1}{3}} N_L \sqrt{n_L} kT\beta_L}{3\Lambda_L}\right)\left(\lambda - \frac{J}{\lambda^2}\right). \tag{7}$$

As noted above, when the short-chain network is stretched, chains in the network break sequentially. Some of the chains become inactive terminal chains, reducing the chain density of the short-chain network, while other chains rearrange into longer chains, leading to increasing numbers of links on a chain of the short-chain network. The damage of the short-chain network can be characterized by the chain alteration model $N_S = N_{S0}\exp[-p(\Lambda_S^{max} - \eta_S^{-1/3})]$, $n_S = n_{S0}\exp[q(\Lambda_S^{max} - \eta_S^{-1/3})]$. Substituting the expressions of N_S and n_S into Eq. (7) and considering that $N_{S0} n_{S0} \nu = 1$ and $N_L n_L \nu = 1$, the nominal stress of the DN gel subjected to uniaxial tension can be given as

$$\frac{s\nu}{kT} = \left(\frac{\eta_S^{\frac{1}{3}}\beta_S}{3\sqrt{n_{S0}}\Lambda_S} exp\left[-\frac{1}{2}p\left(\Lambda_S^{max} - \eta_S^{-\frac{1}{3}}\right)\right] + \frac{\eta_L^{\frac{1}{3}}\beta_L}{3\sqrt{n_L}\Lambda_L}\right)\left(\lambda - \frac{J}{\lambda^2}\right). \tag{8}$$

Given $J = \widehat{J}$, Eq. (8) relates the applied nominal stress s to the stretch λ, yielding instantaneous stress-stretch curves (namely, the instantaneous s-λ curves).

This relation is sketched in Fig. 2 for the representative DN gel with $J = J_0 = 18.05$. At a small stretch, the deformation-induced stiffening of polymer chains dominates, and the stress increases with the stretch. At an intermediate stretch, the damage-induced softening becomes important, and the stress falls as the stretch increases. As the long-chain network approaches its extension limit, the deformation-induced stiffening of long-chain network prevails again, and thus the stress rises again. The shape of the stress-stretch curve indicates a snap-through instability: under monotonic uniaxial tension, during which the tensile force increases rapidly, the DN gel (point 1 in Fig. 2) elongates uniformly in the beginning, and then necking instability suddenly sets in when the applied load reaches the peak value ($\frac{s\nu}{kT} = 9.3 \times 10^{-3}$) of the stress-stretch curve (point 2 in Fig. 2), which determines the critical load for the initiation of necking instability (Zhao, 2012), causing some regions of the gel to thin down more than others (point 3 in Fig. 2). Such necking instability occurs instantaneously once the applied load reaches the critical level, thus we call this type of necking instability the *instant necking instability* and the first peak value of the instantaneous stress-stretch curve the threshold for instant necking instability.

2.3. Delayed necking instability of DN gels

Under a subcritical static load, where a force is rapidly applied and then held at a constant level slightly below the threshold for instant necking instability, delayed necking instability could occur in the DN gel. For example, as shown in Fig. 3(b), when a static subcritical stress $\frac{s\nu}{kT} = 7 \times 10^{-3}$ is applied to the DN gel at time $t = 0$, the gel immediately elongates from the initial free-swelling state [point 1 in Fig. 3(b), $t = 0$] to an instantaneous deformed state [point 2 in Fig. 3(b), $t = 0^+$].

Notably, under constant applied stress $\frac{s\nu}{kT} = 7 \times 10^{-3}$, the instantaneous deformed state denoted by point 2 is not the thermodynamic equilibrium of the open system that consists of the stressed gel and its environment, and the gel will keep swelling by imbibing water to equilibrate with its surroundings and mechanical loads. The nominal principal stresses in the equilibrium state are given by (Ma et al., 2020)

$$s_1 = \frac{\partial W}{\partial \lambda_1} - \frac{\mu}{\nu}\frac{J}{\lambda_1}, \tag{9a}$$

$$s_2 = \frac{\partial W}{\partial \lambda_2} - \frac{\mu}{\nu}\frac{J}{\lambda_2}, \tag{9b}$$

$$s_3 = \frac{\partial W}{\partial \lambda_3} - \frac{\mu}{\nu}\frac{J}{\lambda_3}, \tag{9c}$$

where μ represents chemical potential of water molecules in the environment. Here we assume the DN gel is immersed in pure water, thus $\mu = 0$. Note that the swelling ratio J varies as water molecules migrate in and out of the gel, such that the free energy of mixing W^m is no longer a constant. The total free energy of the DN gel immersed in water takes the form that

$$W = \sum_{i=L,\ S} \eta_i N_i n_i kT \left(\frac{\beta_i}{tanh\beta_i} + \log\frac{\beta_i}{sinh\beta_i} \right) + \frac{kT}{\nu}\left[(J-1)log\frac{J-1}{J} + \sum_{i=L,\ S} \eta_i \chi_i \frac{J-1}{J} \right]. \tag{10}$$

Since the DN gel is subjected to uniaxial tension, we have $s_1 = s$ and $s_2 = s_3 = 0$. Plugging Eq. (10) into Eqs. (9) and considering the chain alteration model described above yield that

$$\left(\frac{\eta_S^{\frac{1}{3}}\beta_S}{3\sqrt{n_{S0}}\Lambda_S} exp\left[-\frac{1}{2}p\left(\Lambda_S^{max} - \eta_S^{-\frac{1}{3}} \right) \right] + \frac{\eta_L^{\frac{1}{3}}\beta_L}{3\sqrt{n_L}\Lambda_L} \right)\lambda_1 + \left[\log\left(1-\frac{1}{J}\right) + \frac{1}{J} + \frac{\chi_S\eta_S + \chi_L\eta_L}{J^2} \right] \frac{J}{\lambda_1} = \frac{s\nu}{kT} \tag{11a}$$

$$\left(\frac{\eta_S^{\frac{1}{3}}\beta_S}{3\sqrt{n_{S0}}\Lambda_S} exp\left[-\frac{1}{2}p\left(\Lambda_S^{max} - \eta_S^{-\frac{1}{3}} \right) \right] + \frac{\eta_L^{\frac{1}{3}}\beta_L}{3\sqrt{L}\Lambda_L} \right)\lambda_2 + \left[\log\left(1-\frac{1}{J}\right) + \frac{1}{J} + \frac{\chi_S\eta_S + \chi_L\eta_L}{J^2} \right] \frac{J}{\lambda_2} = 0. \tag{11b}$$

Given any applied stress s, λ_1 and $\lambda_2 = \lambda_3$ can be solved from Eq. (11), and the swelling ratio J is given by $J = \lambda_1\lambda_2^2$. In Fig. 3(a), we plot the normalized applied stress $\frac{s\nu}{kT}$ as a function of J (i.e., the long-term equilibrium s-J curve). Note that J measures the water content in the gel by $\nu C = J - 1$. The curve reveals a salient feature of hydrogels: a gel under tension tends to absorb more solvents relative to its unstressed state; the higher the tensile stresses, the more solvents the gel can take in. Under the subcritical static stress $\frac{s\nu}{kT} = 7 \times 10^{-3}$, the DN gel can swell from its initial swelling ratio of $J_0 = 18.05$ to $J = 102.75$ by imbibing water [Fig. 3(a)]. Note that this swelling process of gels due to water migration takes time.

It is well-known that gels become more compliant with increasing solvent content, such that, as J increases, the peak value of the instantaneous stress-stretch curve continuously drops [Fig. 3(b)]. After imbibing water and swelling for a while, the gel swells to $J = 33$, presumably at time $t = t_1 > 0$, the peak value of the corresponding stress-stretch curve drops significantly compared to the initial curve with $J = 18.05$, but is still higher than the applied stress level. The DN gel is in an intermediate swollen state [point 3 in Fig. 3(b)] without necking. When the gel continues swelling to $J = 38.62$ at time $t = t_2 > t_1$, the peak value of the stress curve falls to the applied stress level, and the necking instability eventually sets in [point 4 in Fig. 3(b)]. Compared with the instant necking instability

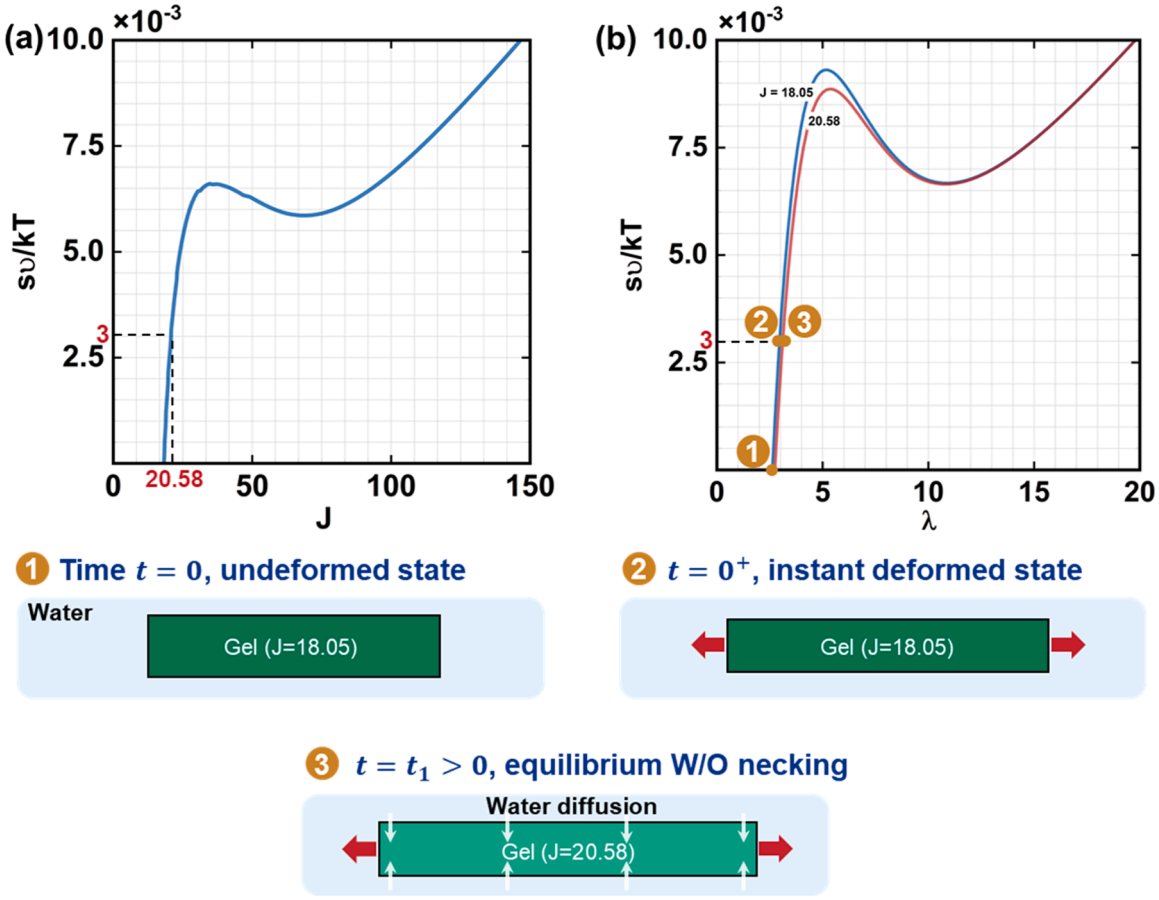

Fig. 4. Equilibrium deformation without necking instability. (a) Under a static stress of $\frac{s_V}{kT} = 3 \times 10^{-3}$, the DN gel can gradually swell, with its swelling ratio J increasing from 18.05 at the free-swelling state to 20.58 at the final equilibrium state. (b) When the DN gel reaches the equilibrium of $J = 20.58$, presumably at time $t = t_1$, the applied stress $\frac{s_V}{kT} = 3 \times 10^{-3}$ is still lower than the peak value of the instantaneous stress-stretch curve. Therefore, the gel eventually reaches an equilibrium state characterized by uniform deformation without necking instability. In the schematics, the change in color from dark green to light green denotes the gradual increase in the water content.

that occurs immediately after a critical load is applied to the DN gel, the necking formation under subcritical loads does not take place until a span of time has elapsed after the static load is applied, and the time-dependent swelling process accounts for the delay in time (from $t = 0$ to $t = t_2$) for the onset of the necking instability. To this end, we call this mode of necking instability the *delayed necking instability*. A critical value of applied stress exists, below which delayed necking instability cannot be triggered (see Appendix C for further discussion), we call this critical value the threshold for delayed necking instability.

Dimensional considerations dictate that the delayed time of the delayed necking instabilities scales with H_0^2/D, where H_0 represents the thickness of the hydrogel bar and D the diffusivity of water molecules. At room temperature, the diffusivity D can be approximated by $D \approx 1 \times 10^{-9}\ m^2 s^{-1}$ (Cheng et al., 2019; Hong et al., 2008; Wang and Hong, 2012). For a hydrogel bar with an initial thickness about $H_0 = 1$ mm, the time required by water molecules to migrate into the hydrogel is on the order of 1000 s, which roughly gives the delayed time scale for the delayed necking instability. Moreover, we would like to emphasize that precise calculation of the delayed time requires a full account of the time-dependent diffusion process by directly solving fully coupled deformation-diffusion equations, which is beyond the scope of this paper and will be studied in the future work.

2.4. Equilibrium deformation without necking instability

When subject to a static stress, $\frac{s_V}{kT} = 3 \times 10^{-3}$ for instance, which is below the threshold for delayed necking instability, the DN gel elongates immediately from the initial free-swelling state [point 1 in Fig. 4(b)] to the instantaneous deformed state [point 2 in Fig. 4 (b)]. Afterward, due to the water absorption driven by the tensile stress, the DN gel imbibes water from the environment and swells. However, when the gel eventually arrives at the equilibrium swelling state of $J = 20.58$ [Fig. 4(a)], the peak-value of the stress-stretch curve for necking instability, which is about 8.9×10^{-3}, still tops the applied stress of $\frac{s_V}{kT} = 3 \times 10^{-3}$ [Fig. 4(b)]. The gel ends up in an equilibrium deformed state without necking formation. That is, necking instability does not take place in DN gels subject to uniaxial

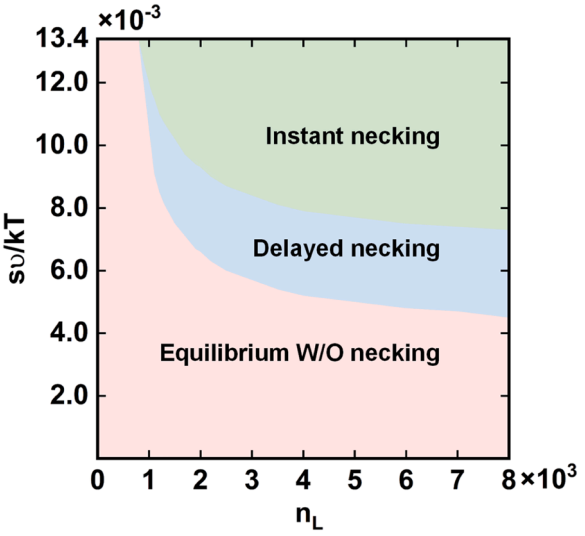

Fig. 5. Regimes of the three modes of necking instability plotted on the plane spanned by two dimensionless parameters: instant necking instability, the equilibrium deformation without necking, and the delayed necking instability mode located in between.

stress that is below the threshold for delayed necking instability.

2.5. A map delineating the three instability modes

The necking instability of DN gels under tension is affected by both the applied load and the material property. For example, the necking instability can be tuned by varying the chain length of the long-chain network (Zhao, 2012). Figure 5 maps the regimes of the three above-mentioned instability modes in the parameter space spanned by the dimensionless applied stress $\frac{s\upsilon}{kT}$ and the dimensionless chain length of the long-chain network n_L. Instant necking instability corresponds to high tensile stresses exceeding the threshold for instant necking instability, while the equilibrium deformation mode prevails for relatively low static stresses below the threshold for delayed necking instability (The procedure for determining the threshold for delayed necking instability is given in Appendix C). These two thresholds define a new regime of delayed necking instability, a new instability mode of hydrogels that has been largely unexplored before.

3. Delayed burst of an inflated spherical hydrogel balloon

3.1. Instant deformation and long-term equilibrium deformation of an inflated hydrogel balloon

Herein, we consider a spherical balloon made of single-network hydrogel which contains only one polymer network and water molecules (Cheng et al., 2019). Take the dry network as the reference state, the free energy of the single-network hydrogel takes the form that

$$W = W^s + W^m = NnkT\left(\frac{\beta}{tanh\beta} + log\frac{\beta}{sinh\beta}\right) + \frac{kT}{\nu}\left[(J-1)\log\left(\frac{J-1}{J}\right) - \frac{\chi}{J}\right], \tag{12}$$

where W^s is the free energy due to stretching the network per reference volume, and W^m is the free energy due to mixing the networks and solvents per reference volume. Moreover, N is the number of polymer chains per reference volume, n the number of freely jointed links on a polymer chain, kT the temperature in the unit of energy, ν the volume of the water molecule, χ the dimensionless measure of the strength of pairwise interactions between water molecules and monomers of the single network. $\beta = L^{-1}(\Lambda/\sqrt{n})$, where $L^{-1}(x)$ is the inverse Langevin function and Λ is the stretch of individual polymer chain. When subjected to an internal pressure, the deformation of the balloon can be characterized by stretches λ_θ, λ_ϕ and λ_r in the spherical coordinate system. Then $\Lambda = \sqrt{\frac{\lambda_\theta^2+\lambda_\phi^2+\lambda_r^2}{3}}$ and the swelling ratio of the gel $J = \lambda_\theta\lambda_\phi\lambda_r$.

(i) Instant deformation of the hydrogel balloon

When the internal pressure is applied rapidly, the instant deformation of the balloon wall is volume-conserved because the short time interval does not allow water migration in and out of the gel. Therefore, during the instantaneous deformation, the swelling ratio of the wall of the hydrogel balloon remains unchanged, i.e., $J = \widehat{J}$ ($\widehat{J}$ represents a constant). Following the derivation in Section 2.2, we

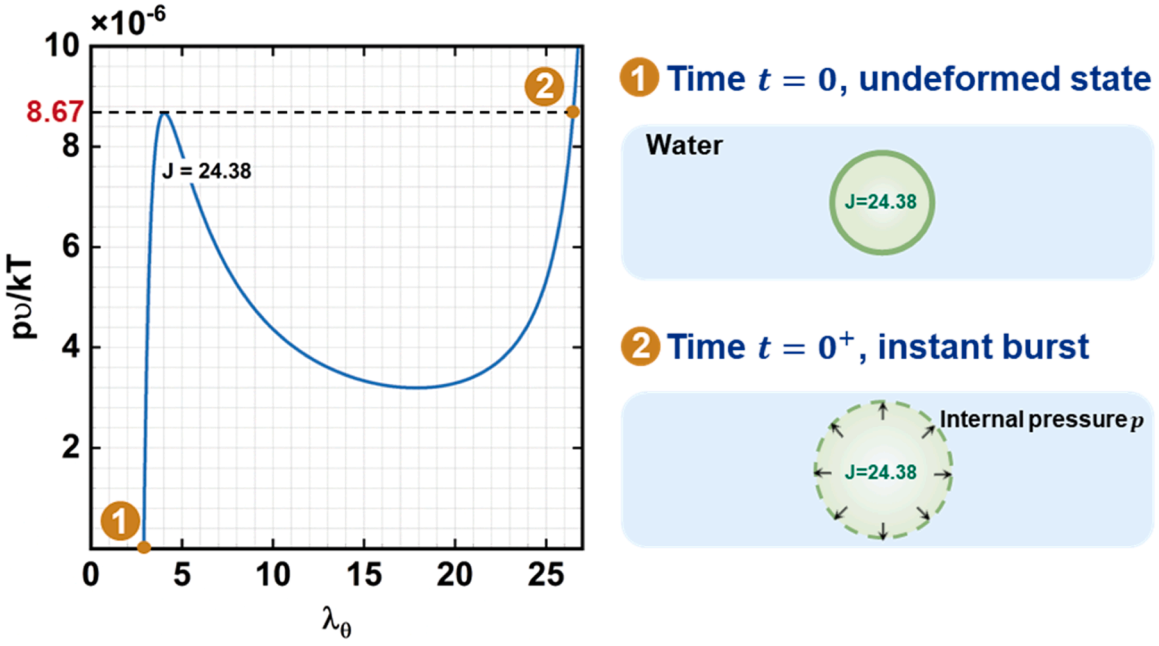

Fig. 6. The instantaneous pressure-stretch curve (p-λ_θ curve). Instant burst instability of a hydrogel balloon takes place when the rapidly applied pressure p reaches the peak value of the curve. In the schematics, the intact balloon wall is illustrated as solid lines, while the fractured balloon wall as a consequence of the burst instability is sketched as dashed lines.

can modify the free energy function W of the hydrogel balloon by imposing the incompressibility condition and taking into account that $J = \widehat{J}$ is a constant, as follows,

$$\widehat{W} = NnkT\left(\frac{\beta}{tanh\beta} + log\frac{\beta}{sinh\beta}\right) + \Pi(J - \widehat{J}), \tag{13}$$

where Π denotes a Lagrange multiplier. Note that the free energy of mixing W^m has been neglected in Eq. (13) since it becomes a constant when J is fixed and does not contribute to the mechanical stresses.

In response to an internal pressure p, the balloon deforms in a spherically symmetric fashion, such that $\sigma_\theta = \sigma_\phi$, and $\lambda_\theta = \lambda_\phi$. Considering $\sigma_i = \frac{\partial \widehat{W}}{\partial \lambda_i}\frac{\lambda_i}{J}$ $(i = r,\ \theta, \phi)$, $Nn\nu = 1$ (i.e., the dry polymer network itself is also incompressible), and $J = \lambda_r\lambda_\theta^2$, we obtain Cauchy stresses as

$$\sigma_\theta = \sigma_\phi = \frac{\lambda_\theta}{J}\frac{\partial W}{\partial \lambda_\theta} + \Pi = \frac{kT}{\nu}\frac{\beta}{3\sqrt{n}\Lambda}\frac{\lambda_\theta^2}{J} + \Pi, \tag{14-1}$$

$$\sigma_r = \frac{\lambda_r}{J}\frac{\partial W}{\partial \lambda_r} + \Pi = \frac{kT}{\nu}\frac{\beta}{3\sqrt{n}\Lambda}\frac{J}{\lambda_\theta^4} + \Pi. \tag{14-2}$$

When inflated by the internal pressure p, Cauchy stresses in the radial and hoop directions are

$$\sigma_\theta = \frac{pr}{2h}, \tag{15-1}$$

$$\sigma_r = 0, \tag{15-2}$$

where r and h are the radius and the thickness of the balloon in the deformed state, respectively. Combining Eqs. (14) and (15) yields that

$$\frac{pr}{2h} = \frac{kT}{\nu}\frac{\beta}{3\sqrt{n}\Lambda}\left(\frac{\lambda_\theta^2}{J} - \frac{J}{\lambda_\theta^4}\right). \tag{16}$$

Let R and H be the radius and the thickness of the hydrogel balloon in the reference state. The hoop stretch λ_θ and radial stretch λ_r can be given by $\lambda_\theta = \frac{r}{R}$ and $\lambda_r = \frac{h}{H}$. Plugging the expressions of λ_θ and λ_r into Eq. (16) leads to

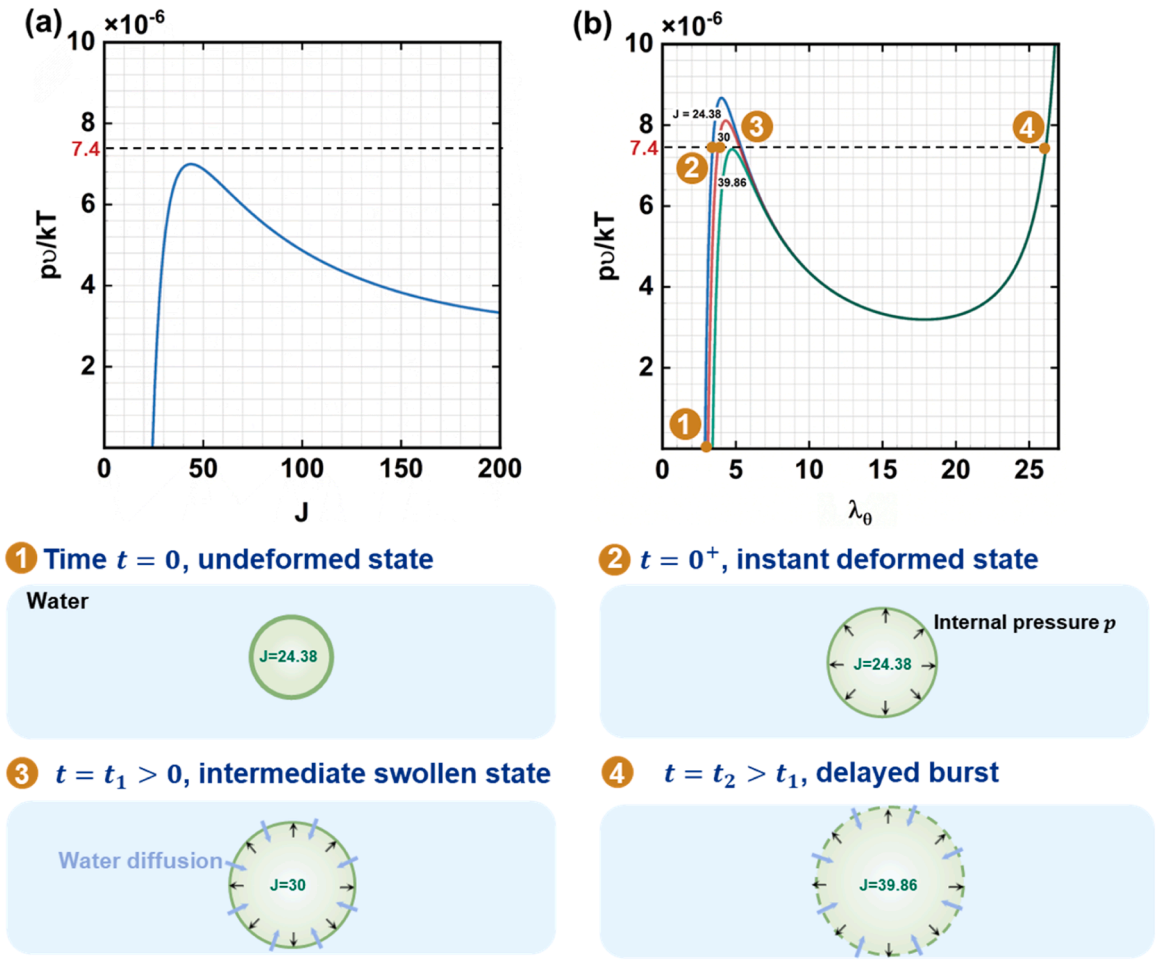

Fig. 7. . Delayed burst instability of a hydrogel balloon. (a) The equilibrium pressure-swelling curve (i.e., the equilibrium p-J curve), which gives the long-term equilibrium swelling ratio corresponding to an applied pressure. (b) The instantaneous pressure-stretch curve (i.e., the instantaneous p-λ_θ curve), which describes the instantaneous response of the gel balloon at a given swelling ratio J. As the gel takes in water and swells with increasing J, delayed burst occurs once the peak value of the p-λ_θ curve reduces to the applied pressure level.

$$\frac{p\nu}{kT}=\frac{2H}{R}\frac{\beta}{3\sqrt{n}\Lambda}\left(\frac{1}{\lambda_\theta}-\frac{J^2}{\lambda_\theta^7}\right). \tag{17}$$

Based on Eq. (17), instantaneous pressure-stretch curves (namely, the p-λ_θ curve) shown in Fig. 6-8 are sketched.

(ii) Long-term equilibrium deformation of the hydrogel balloon

When the hydrogel balloon is subjected to a static internal pressure p for a prolonged period, the hydrogel will imbibe water slowly and swell continuously, eventually equilibrating with the mechanical load and the environment in the long term. The long-term equilibrium response of the hydrogel balloon can be obtained by using $\sigma_i=\frac{\partial W}{\partial\lambda_i}\frac{\lambda_i}{J}$ $(i=r,\ \theta,\ \phi)$. It is worthwhile to mention that W takes the form given by Eq. (12) and the swelling ratio $J=\lambda_\theta^2\lambda_r$ is no longer a constant in this scenario. It follows that the corresponding hoop and radial Cauchy stress components are

$$\sigma_\theta=\sigma_\phi=\frac{\partial W}{\partial\lambda_\theta}\frac{\lambda_\theta}{J}=\frac{kT}{\nu}\frac{\beta}{3\sqrt{n}\Lambda}\frac{\lambda_\theta^2}{J}+\frac{kT}{\nu}\left[log\left(1-\frac{1}{J}\right)+\frac{1}{J}+\frac{\chi}{J^2}\right], \tag{18a}$$

$$\sigma_r=\frac{\partial W}{\partial\lambda_r}\frac{\lambda_r}{J}=\frac{kT}{\nu}\frac{\beta}{3\sqrt{n}\Lambda}\frac{J}{\lambda_\theta^4}+\frac{kT}{\nu}\left[log\left(1-\frac{1}{J}\right)+\frac{1}{J}+\frac{\chi}{J^2}\right]. \tag{18b}$$

By substituting Eqs. (18) into Eqs. (15), we obtain

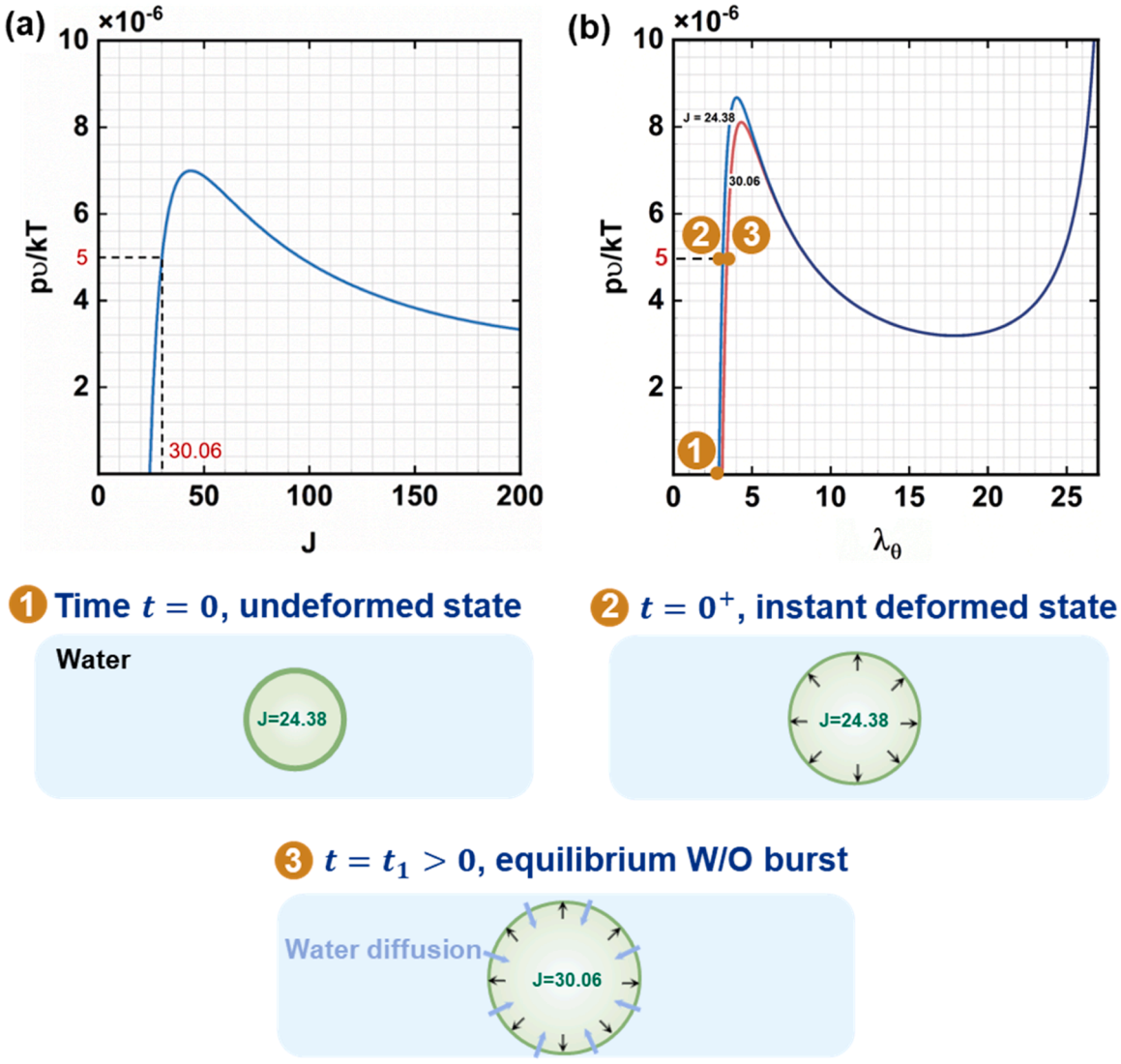

Fig. 8. Equilibrium deformation without burst instability. (a) The equilibrium p-J curve. Under a static internal pressure $\frac{p\nu}{kT} = 5 \times 10^{-6}$, the hydrogel can swell from $J = 24.38$ to 30.06. (b) The instantaneous p-λ curves. It shows that the hydrogel balloon ends up with an equilibrium deformation state without burst instability.

$$\frac{p\nu}{kT} = \frac{2H\lambda_r}{R\lambda_\theta}\left(\frac{\beta}{3\sqrt{n}\Lambda}\frac{\lambda_\theta^2}{J} + \left[log\left(1-\frac{1}{J}\right)+\frac{1}{J}+\frac{\chi}{J^2}\right]\right), \tag{19a}$$

$$\frac{kT}{\nu}\frac{\beta}{3\sqrt{n}\Lambda}\frac{J}{\lambda_\theta^4} + \frac{kT}{\nu}\left[log\left(1-\frac{1}{J}\right)+\frac{1}{J}+\frac{\chi}{J^2}\right] = 0 \tag{19b}$$

Given an internal pressure p, the equilibrium swelling ratio J and hoop stretch λ_θ can be calculated by solving Eqs. (19) – note that $\lambda_r = J/\lambda_\theta^2$. Then, the equilibrium pressure-swelling curves (i.e., the equilibrium p-J curve) provided in Fig. 7 and 8 can be obtained. Moreover, setting $p = 0$ gives the initial swelling ratio J_0 of the hydrogel balloon before any internal pressure is applied.

3.2. *The three instability modes of the inflated spherical hydrogel balloon*

In this section, the following values are used for the single-network hydrogel balloon: $n = 500$ (Zhao, 2012), $\chi = 0.1$ (Hong et al., 2009), $H/R = 1/100$ (Cheng et al., 2019). The rationale for these specified chosen values is as follows: for hydrogels, the parameter n – i.e., number of links per chain – varies approximately between 10 and 5000 (Zhao, 2012). For instance, according to Zhao et al. (Zhao, 2012), n is set to 50 for short-chain networks and 2000 for long-chain networks, respectively. Herein, we take $n = 500$ accordingly.

From another perspective, the dimensionless crosslinking density $N\nu$ of hydrogels may be in the range of $1 \times 10^{-4} \sim 1 \times 10^{-1}$ (Hong et al., 2009). Herein, we choose $N\nu$ to be 2×10^{-3}. Taking into account the volume conservation condition of $nN\nu = 1$, n is calculated to be 500. Moreover, the value of parameter χ is typically in the range of $0 \sim 1.2$ (Hong et al., 2009). Following Hong et al., we choose χ to be 0.1. For the thickness-to-radius ratio H/R, a value of 1/100 which is typical for thin-walled balloons is used (Cheng et al., 2019). Given these values, the initial swelling ratio of the hydrogel balloon is $J_0 = 24.38$. We find there exists a delayed instability mode for the burst instability of hydrogel balloons.

(i) *Instant burst instability*.

When an internal pressure p is applied rapidly, the hydrogel balloon deforms instantaneously, with the swelling ratio J remaining to be 24.38. Fig. 6 sketches the instantaneous pressure-stretch curve (p-λ_θ curve), where the peak pressure value is $\frac{p\nu}{kT} = 8.67 \times 10^{-6}$. When the internal pressure reaches the critical level (i.e., the peak value of the p-λ_θ curve), snap-through instability occurs instantaneously, often causing the burst of the hydrogel balloon. Such a phenomenon is called instant burst instability.

(ii) *Delayed burst instability*.

Suppose a subcritical static internal pressure $\frac{p\nu}{kT} = 7.4 \times 10^{-6}$ is applied to the hydrogel balloon. The burst instability will not occur because the peak value ($\frac{p\nu}{kT} = 8.67 \times 10^{-6}$) of the instantaneous p-λ_θ curve at $J = 24.38$ is higher than the applied pressure, as evident from Fig. 7(b). Fig. 7(a) plots the equilibrium pressure-swelling curve (i.e., equilibrium p-J curve), which characterizes the long-term equilibrium deformation of the hydrogel balloon in response to the static internal pressure and is obtained by solving Eqs. (19). The p-J curve shows that, under a static internal pressure of $\frac{p\nu}{kT} = 7.4 \times 10^{-6}$, the hydrogel balloon will absorb water unboundedly. Consequently, as the swelling ratio J increases due to water absorption, the hydrogel softens and the peak value of the instantaneous p-λ_θ curve decreases [Fig. 7(b)]. When the swelling ratio rises to $J = 39.86$, the peak value of the instantaneous p-λ_θ curve drops to the applied pressure level, thereby leading to the burst instability. Owing to the fact that it takes a period of time for the gel to imbibe water and increase its swelling ratio from 24.38 to 39.86, we call such instability taking place after a time of delay as the delayed burst instability of hydrogel balloon.

(iii) *Equilibrium deformation without burst instability*.

When we apply a relatively low internal pressure, e.g., $\frac{p\nu}{kT} = 5 \times 10^{-6}$, to the hydrogel balloon, the pressure is not sufficiently large to trigger the instant burst instability; The gel balloon will take in water and swell, with its swelling ratio J increasing from 24.38 at the initial free-swelling state to 30.06 at the equilibrium state [Fig. 7(a)]. Note that the peak value of the instantaneous p-λ_θ curve with $J = 30.06$ is $\frac{p\nu}{kT} = 8.1 \times 10^{-6}$, higher than the applied pressure. That is, the applied pressure cannot induce the delayed instability as well. The hydrogel balloon ends up with an equilibrium deformation state without burst instability.

4. Delayed bulging of a pressurized cylindrical hydrogel tube

4.1. Instant deformation and long-term equilibrium deformation of a pressurized cylindrical hydrogel tube

In this section, we consider a cylindrical hydrogel tube made of a single-network hydrogel, of which the free energy function takes the same form as that used in Section 3 [Equation (12)]. When the cylindrical tube is inflated by a uniform internal pressure p, it expands by stretches λ_θ, λ_r and λ_z. Thus $\Lambda = \sqrt{\frac{\lambda_\theta^2+\lambda_r^2+\lambda_z^2}{3}}$ and the swelling ratio of the gel $J = \lambda_\theta\lambda_r\lambda_z$.

(i) *Instant deformation of a pressurized cylindrical hydrogel tube*

The hydrogel tube is subjected to an internal pressure p and a dead weight F hanging below, as illustrated in Fig. 1(c). As extensively discussed above, the instantaneous deformation of the hydrogel is volume-conserving, with a constant swelling ratio $J = \widehat{J}$. To this end, by taking into account the incompressibility condition (i.e., $J = \widehat{J}$), we can recast the free energy function (12) in the form that

$$\widehat{W} = NnkT\left(\frac{\beta}{tanh\beta} + log\frac{\beta}{sinh\beta}\right) + \Pi(J - \widehat{J}), \tag{20}$$

where Π is a Lagrange multiplier.

The Cauchy stresses can be calculated by $\sigma_i = \frac{\partial\widehat{W}}{\partial\lambda_i}\frac{\lambda_i}{J}$ $(i = r,\ \theta, z)$. By considering that $Nn\nu = 1$ and $J = \lambda_r\lambda_\theta\lambda_z$, the expressions of Cauchy stresses are given by

$$\sigma_\theta = \frac{\lambda_\theta}{J}\frac{\partial W}{\partial\lambda_\theta} + \Pi = \frac{kT}{\nu}\frac{\beta}{3\sqrt{n}\Lambda}\frac{\lambda_\theta^2}{J} + \Pi, \tag{21a}$$

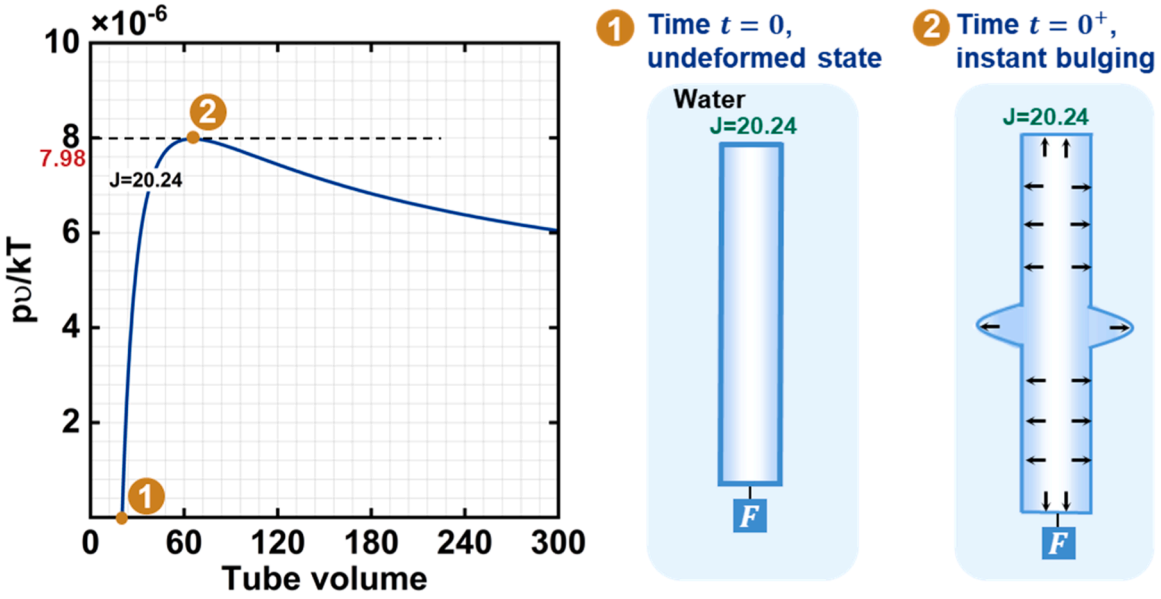

Fig. 9. The instantaneous pressure-volume curve (p-$\lambda_\theta^2\lambda_z$ curve). Instant bulging instability of a pressurized cylindrical hydrogel tube takes place when the applied pressure reaches the peak value of the curve.

$$\sigma_r = \frac{\lambda_r}{J}\frac{\partial W}{\partial \lambda_r} + \Pi = \frac{kT}{\nu}\frac{\beta}{3\sqrt{n}\Lambda}\frac{\lambda_r^2}{J} + \Pi. \tag{21b}$$

$$\sigma_z = \frac{\lambda_r}{J}\frac{\partial W}{\partial \lambda_z} + \Pi = \frac{kT}{\nu}\frac{\beta}{3\sqrt{n}\Lambda}\frac{\lambda_z^2}{J} + \Pi. \tag{21c}$$

When subjected to an internal pressure p, radial and hoop stresses in the gel are

$$\sigma_\theta = \frac{pr}{h}, \tag{22a}$$

$$\sigma_r = 0, \tag{22b}$$

where r and h are the radius and the thickness of the tube in the current configuration, respectively. Combining Eqs. (21) and (22), we can obtain the expression of the internal pressure p as

$$\frac{p\nu}{kT} = \frac{h}{r}\frac{\beta}{3\sqrt{n}\Lambda}\left(\frac{\lambda_\theta^2}{J} - \frac{\lambda_r^2}{J}\right) \tag{23}$$

Here $r = \lambda_\theta R$ and $h = \lambda_r H$, where R and H are the radius and the thickness of the hydrogel tube in the reference state (i.e., the dry polymer network). We can recast the internal pressure p in the form that

$$\frac{p\nu}{kT} = \frac{H}{R}\frac{\beta}{3\sqrt{n}\Lambda}\frac{1}{\lambda_\theta^2\lambda_z}\left(\lambda_\theta^2 - \lambda_r^2\right). \tag{24}$$

Note that a dead weight F is hanging below the gel tube. Therefore, the force balance along z direction (namely, the longitudinal direction of the tube) gives that

$$\sigma_z = \frac{p\pi r^2 + F}{2\pi rh}. \tag{25}$$

By replacing r and h with $r = \lambda_\theta R$ and $h = \lambda_r H$, Eq. (25) can be rewritten as

$$\frac{\sigma_z\nu}{kT} = \frac{R}{2H}\frac{\lambda_\theta}{\lambda_r}\frac{\nu p}{kT} + \frac{1}{\lambda_\theta\lambda_r}\frac{s_{applied}\nu}{kT} \tag{26}$$

where $s_{applied} = \frac{F}{2\pi RH}$ is the applied nominal stress by the dead weight F along the z direction. By subtracting Eq. (21b) from Eq. (21c) and taking into account that $\sigma_r = 0$, σ_z can also be expressed as

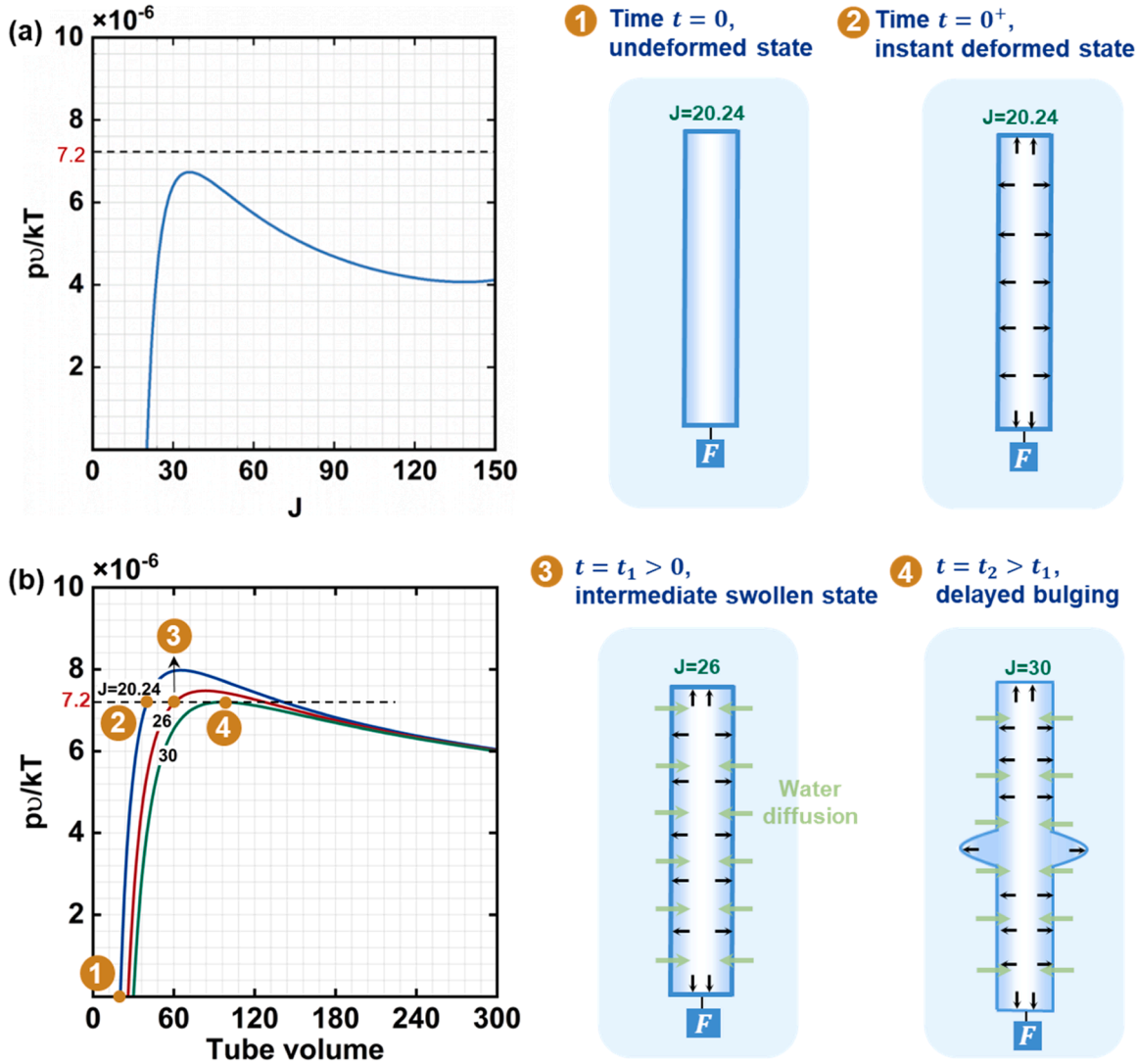

Fig. 10. Delayed bulging instability of a hydrogel tube. (a) The equilibrium pressure-volume curve (i.e., the equilibrium p-J curve). It indicates that a hydrogel tube subjected to an internal pressure of $\frac{p\nu}{kT} = 7.2 \times 10^{-6}$ will gradually absorb water and swell with increasing swelling ratio J. (b) The instantaneous pressure-volume curves (i.e., the instantaneous p-$\lambda_\theta^2\lambda_z$ curve), which describe the instantaneous response of the gel tube at a given swelling ratio J. Note that the peak value of the instantaneous pressure-volume curve corresponds to the bulging initiation. As the gel takes in water and swells with increasing J, delayed burst occurs once the peak value of the p-λ_θ curve reduces to the applied pressure level.

$$\frac{\sigma_z\nu}{kT} = \frac{\sigma_z\nu}{kT} - \frac{\sigma_r\nu}{kT} = \frac{\beta}{3\sqrt{n}\Lambda}\left(\frac{\lambda_z^2}{J} - \frac{\lambda_r^2}{J}\right). \tag{27}$$

Combining Eq. (26) and Eq. (27) yields that

$$\frac{R}{2H}\frac{\lambda_\theta}{\lambda_r}\frac{p\nu}{kT} + \frac{1}{\lambda_\theta\lambda_r}\frac{s_{applied}\nu}{kT} = \frac{\beta}{3\sqrt{n}\Lambda}\left(\frac{\lambda_z^2}{J} - \frac{\lambda_r^2}{J}\right) \tag{28}$$

Plugging Eq. (24) into Eq. (28), we can obtain the equation

$$\frac{1}{2}\frac{\beta}{3\sqrt{n}\Lambda}\frac{1}{\lambda_z}\left(\lambda_\theta^2 - \lambda_r^2\right) + \frac{s_{applied}\nu}{kT} = \frac{\beta}{3\sqrt{n}\Lambda}\frac{1}{\lambda_z}\left(\lambda_z^2 - \lambda_r^2\right). \tag{29}$$

For a hydrogel balloon with a constant swelling ratio $J = \lambda_\theta\lambda_r\lambda_z = \widehat{J}$, given an internal pressure p and dead weight F, the stretches λ_θ, λ_r and λ_z can be determined by solving Eqs. (24) and (29). Accordingly, instantaneous pressure-volume curves (i.e., instantaneous p-$\lambda_\theta^2\lambda_z$ curves) shown in Figs. 9-11 can be obtained. One notes that $\lambda_\theta^2\lambda_z$ describes the change of volume enclosed by the hydrogel tube,

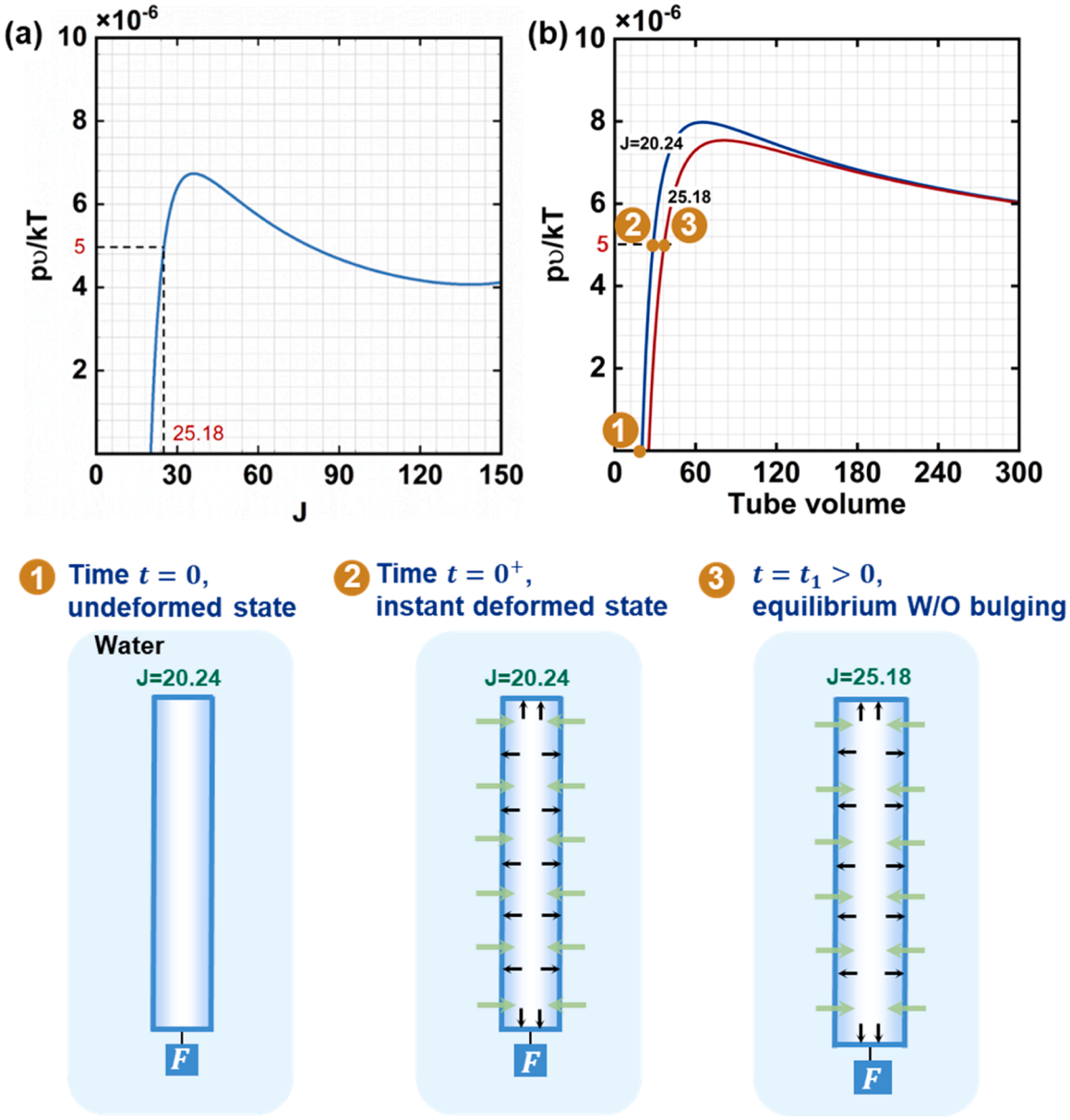

Fig. 11. Equilibrium deformation without bulging instability. (a) The equilibrium p-J curve. Under a static internal pressure $\frac{p\upsilon}{kT} = 5 \times 10^{-6}$, the hydrogel can swell from $J = 20.24$ to 25.18. (b) The instantaneous p-λ curves. It shows that the bulging of hydrogel tube does not occur under the internal pressure $\frac{p\upsilon}{kT} = 5 \times 10^{-6}$.

and the peak value of the instantaneous p-$\lambda_\theta^2\lambda_z$ curve determines the critical stress at which the bulging process initiates (Chater and Hutchinson, 1984).

(ii) *Long-term equilibrium deformation of a pressurized cylindrical hydrogel tube*

Driven by the internal pressure p and the dead weight F, the long-term deformation of the hydrogel tube is accompanied by water absorption, until the entire system consisting of the gel, the mechanical loads and the water reservoir reaches an equilibrium, such that the swelling ratio J is not anymore a constant. Using the free energy given by Eq. (12), we can derive the Cauchy stresses as follows

$$\frac{\nu\sigma_\theta}{kT} = \frac{\partial W}{\partial \lambda_\theta}\frac{\lambda_\theta}{J} = \frac{\beta}{3\sqrt{n}\Lambda}\frac{\lambda_\theta^2}{J} + \left[log\left(1-\frac{1}{J}\right) + \frac{1}{J} + \frac{\chi}{J^2}\right], \tag{30a}$$

$$\frac{\nu\sigma_r}{kT}=\frac{\partial W}{\partial\lambda_r}\frac{\lambda_r}{J}=\frac{\beta}{3\sqrt{n}\Lambda}\frac{\lambda_r^2}{J}+\left[log\left(1-\frac{1}{J}\right)+\frac{1}{J}+\frac{\chi}{J^2}\right], \tag{30b}$$

$$\frac{\nu\sigma_z}{kT}=\frac{\partial W}{\partial\lambda_z}\frac{\lambda_z}{J}=\frac{\beta}{3\sqrt{n}\Lambda}\frac{\lambda_z^2}{J}+\left[log\left(1-\frac{1}{J}\right)+\frac{1}{J}+\frac{\chi}{J^2}\right]. \tag{30c}$$

Combining Eqs. (22), (25) and Eqs. (30) yields that

$$\frac{p\nu}{kT}=\frac{H\lambda_r}{R\lambda_\theta}\left(\frac{\beta}{3\sqrt{n}\Lambda}\frac{\lambda_\theta^2}{J}+\left[log\left(1-\frac{1}{J}\right)+\frac{1}{J}+\frac{\chi}{J^2}\right]\right), \tag{31a}$$

$$\frac{\beta}{3\sqrt{n}\Lambda}\frac{\lambda_r^2}{J}+\left[log\left(1-\frac{1}{J}\right)+\frac{1}{J}+\frac{\chi}{J^2}\right]=0, \tag{31b}$$

$$\frac{R}{2H}\frac{\lambda_\theta}{\lambda_r}\frac{\nu p}{kT}+\frac{1}{\lambda_\theta\lambda_r}\frac{s_{applied}\nu}{kT}=\frac{\beta}{3\sqrt{n}\Lambda}\frac{\lambda_z^2}{J}+\left[log\left(1-\frac{1}{J}\right)+\frac{1}{J}+\frac{\chi}{J^2}\right]. \tag{31c}$$

When the applied pressure p and the dead weight F are known, λ_θ, λ_r, and λ_z can be determined by solving Eqs. (31), which gives the long-term equilibrium pressure-swelling curve (i.e., the equilibrium p-J curve) shown in Fig. 10 and 11.

Herein, we refer to the state, in which the gel tube equilibrates with the given dead weight F and the water reservoir ($p=0$), as the initial state. The corresponding initial swelling ratio J_0 can be calculated by setting $p=0$ in Eqs. (31).

4.2. Three instability modes of the pressurized cylindrical hydrogel tube

When analyzing the instability modes of the pressurized cylindrical gel tube, we take the following values: $n=300$ (Zhao, 2012), $\chi=0.1$ (Hong et al., 2009), $H/R=1/100$ (Cheng et al., 2019), $s_{applied}\nu/kT=5\times10^{-3}$. The corresponding initial free-swelling ratio of the hydrogel is $J_0=20.24$. We will show that the delayed instability mode also exists for the bulging instability of pressurized cylindrical hydrogel tubes.

(i) *Instant bulging instability*

When an internal pressure p that increases rapidly is applied to the hydrogel tube, the tube expands and elongates instantaneously, with the swelling-ratio J remaining at its initial value of 20.24, without any water uptake. Once the pressure p increases to the peak value ($\frac{p\nu}{kT}=7.98\times10^{-6}$) of the instantaneous pressure-volume curve (p-$\lambda_\theta^2\lambda_z$ curve) shown in Fig. 9, bulging instability of the tube takes place. Since the bulging occurs immediately when the pressure reaches the critical level, such instability mode is termed instant bulging instability.

(ii) *Delayed bulging instability*.

If an internal pressure $\frac{p\nu}{kT}=7.2\times10^{-6}$, which does not exceed the peak value ($\frac{p\nu}{kT}=7.98\times10^{-6}$) of the initial instantaneous p-$\lambda_\theta^2\lambda_z$ curve, is applied to the gel tube, instant bulging does not occur. Then the gel tube will gradually take in water molecules and swell in response to the static internal pressure $\frac{p\nu}{kT}=7.2\times10^{-6}$, as shown in Fig. 10(a). As a consequence, the peak value of the instantaneous p-$\lambda_\theta^2\lambda_z$ curve continuously decreases as the swelling ratio of the hydrogel tube increases [Fig. 10(b)]. Till the swelling ratio reaches $J=30.0$, the peak value of the instantaneous p-$\lambda_\theta^2\lambda_z$ curve drops to the static internal pressure level $\frac{p\nu}{kT}=7.2\times10^{-6}$, leading to the onset of the bulging instability. Because the bulging does not occur until a span of time has eclipsed after the internal pressure is applied, we define such instability mode as the delayed bulging instability.

(iii) *Equilibrium deformation without bulging instability*.

Now we consider the deformation of hydrogel tube subjected to a low internal pressure. Take $\frac{p\nu}{kT}=5\times10^{-6}$ as an example. Instant bulging instability does not occur and the gel tube keeps expanding by imbibing water until the swelling ratio J reaches 25.18 [Fig. 11 (a)]. At this moment, the peak value of the instantaneous p-$\lambda_\theta^2\lambda_z$ curve $\frac{p\nu}{kT}$ equals to 7.54×10^{-6}, still higher than the applied internal pressure $\frac{p\nu}{kT}=5\times10^{-6}$. Consequently, the applied internal pressure $\frac{p\nu}{kT}=5\times10^{-6}$ is unable to trigger the bulging instability. That is, the gel tube will end up with the equilibrium deformation without bulging instability.

5. Universality of delayed tensile instabilities

As discussed above, the delayed instability mode of hydrogels is not limited to necking, but is universal for many types of instabilities that are triggered by tensile stresses, including necking instability of the stretched DN gel, burst of a pressurized hydrogel balloon, and bulging of an inflated hydrogel tube. The underlying physics are as follows: (1) The onset of all types of tensile instabilities

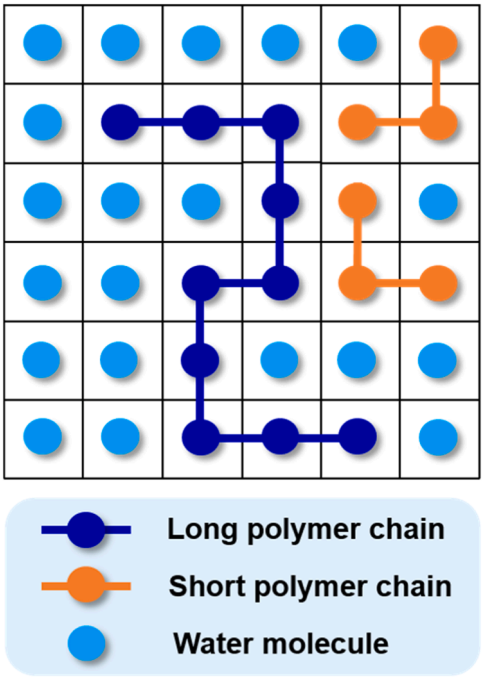

Fig. A1. A liquid lattice model in which long polymer chains and short polymer chains are allocated in water. It is assumed the monomers and water molecules are identical in size (Flory, 1953).

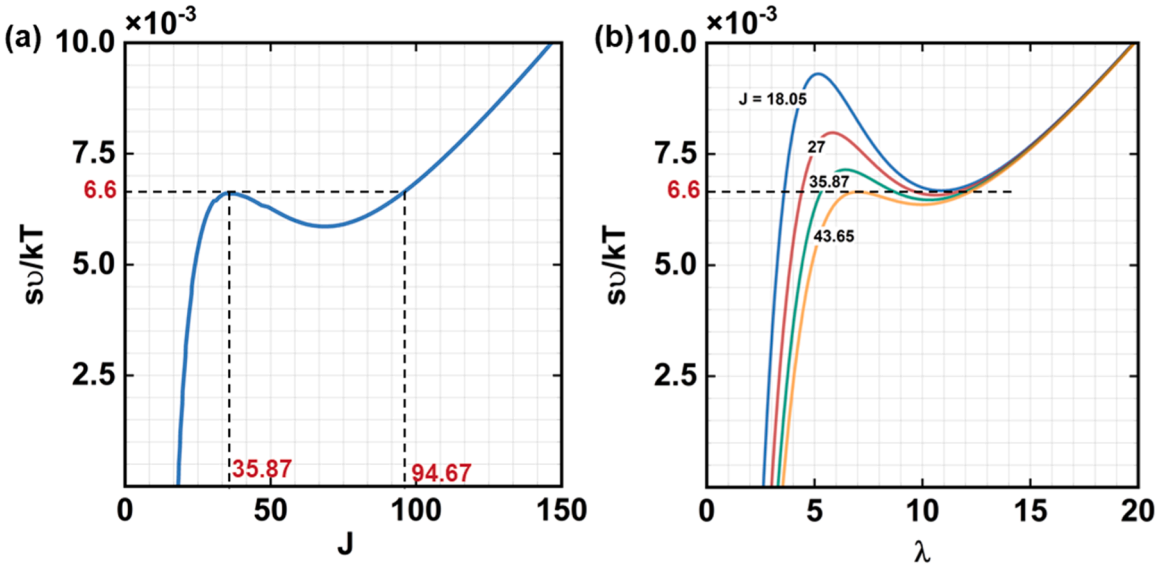

Fig. C1. The long-term equilibrium deformation and instantaneous mechanical response of DN gels under uniaxial tension. Herein, $n_L = 2000$. (a) The equilibrium stress-volume curve (i.e., the equilibrium *s*-*J* curve), which relates the long-term equilibrium swelling ratio to applied stress. (b) The instantaneous stress-stretch curve (i.e., the instantaneous *s*-λ curve), which describes the instantaneous response of DN gels with a given swelling ratio *J*.

of hydrogels mentioned above is linked to a critical load above which the instability occurs (e.g., the peak value of the instantaneous stress-stretch curve for example). This critical load, apparently, scales with the modulus of the hydrogel. (2) One salient feature of hydrogels is that, when subject to a tensile stress, hydrogel swells by imbibing more water relative to its unstressed free-swelling state. The increase in water content reduces the number of polymer chains per volume of the gel, thereby lowering the gel modulus as well as the threshold for instantaneous instability. (3) When a subcritical tensile load, which is slightly below the threshold for instant instability, is applied to the hydrogel structure, the water absorption driven by tensile stresses causes a gradual decrease in the critical

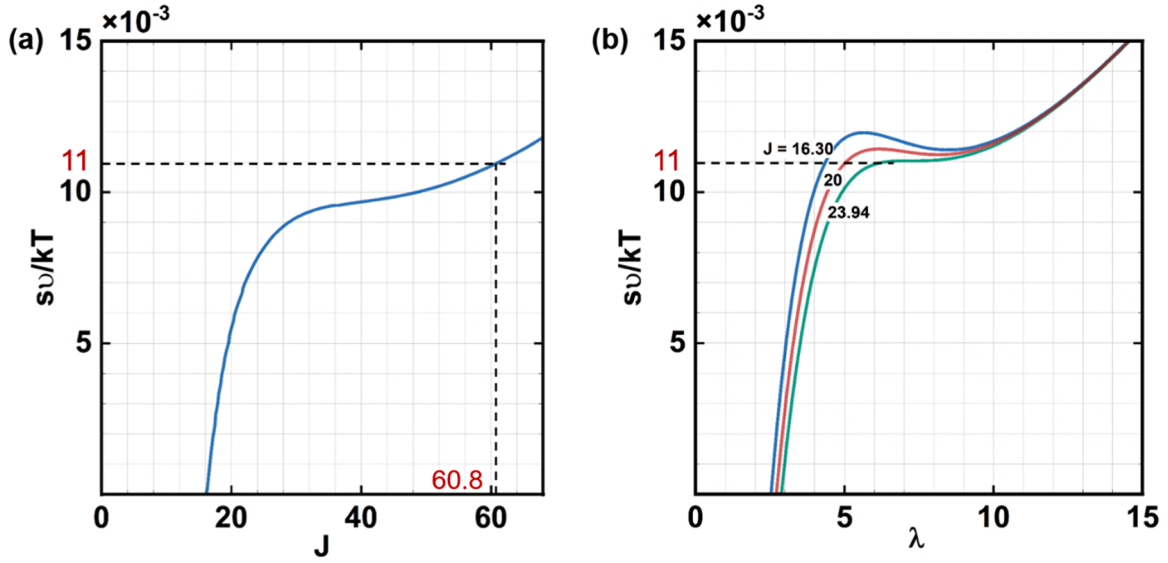

Fig. C2. The long-term equilibrium deformation and instantaneous mechanical response of DN gels under uniaxial tension. Herein, $n_L = 1000$. (a) The equilibrium stress-swelling curve (i.e., the equilibrium *s*-*J* curve). (b) The instantaneous stress-stretch curves (i.e., the instantaneous *s*-λ curve).

load for triggering the delayed instability. Consequently, the delayed instability mode becomes inevitable when the critical load for instability drops to the applied load level.

It is worthwhile to note that instability triggered by compression (e.g., creasing of hydrogels) is unlikely to occur in a delayed fashion. When a subcritical compressive load is applied to a hydrogel, the structure remains stable and loses water, giving rise to an increased critical load for the instability, such that the critical load can never drop to the applied load level. That is, tension is a necessary condition for delayed instabilities of hydrogels. In this regard, the delayed instabilities analyzed in this work are called delayed tensile instability to underline the fact that only instabilities of hydrogels triggered by tensile stresses can have a delayed mode.

6. Conclusion

In this work, we theoretically uncover a new instability mode that has remained largely unstudied before: the delayed tensile instability of hydrogels. Most existing studies concern instant instabilities that occur instantaneously when the applied load reaches a critical level. In stark contrast, the delayed tensile instability, as the name suggests, does not take place until a period has elapsed after a static load is applied. The cause of the delayed tensile instability of hydrogels is attributed to the time-dependent swelling process of hydrogels induced by tension.

The delayed tensile instabilities are counterintuitive as they are triggered by loads below the threshold for the well-known instant instability. Such an anomalous instability mode may occur in functional hydrogel structures such as artificial cartilage, which are in contact with water in the environment and subjected to prolonged mechanical loads. Given its latent nature, the delayed instability mode could be more detrimental than the instant instability mode. The results from this study shed light on guidelines in designing hydrogels to mitigate such a delayed instability. On the other hand, a better understanding of the delayed instability could potentially enable design of new applications to harness such a less unstudied instability. We call for further experiments to explore such opportunities.

CRediT authorship contribution statement

Jie Ma: Formal analysis, Investigation, Data curation, Writing – original draft. **Daochen Yin:** Formal analysis. **Zhi Sheng:** Formal analysis. **Jian Cheng:** Formal analysis. **Zheng Jia:** Conceptualization, Methodology, Investigation, Resources, Writing – review & editing, Supervision, Funding acquisition. **Teng Li:** Conceptualization, Writing – review & editing, Supervision. **Shaoxing Qu:** Resources, Writing – review & editing, Supervision.

Declaration of Competing Interest

The authors declare that they have no known competing financial interests or personal relationships that could have appeared to influence the work reported in this paper.

Data Availability

Data will be made available on request.

Acknowledgements

This work is supported by the National Natural Science Foundation of China (Grant Nos. 11802269 and 12072314), Natural Science Foundation of Zhejiang Province (Grant No. LR22A020005), and the 111 Project (Grant No. B21034).

Appendix A. The derivation of the free energy of mixing W^m for DN gels

Based on the liquid lattice model developed by Flory and Huggins, we derive the free energy of mixing of the double-network hydrogel (DN gel). As shown in Fig. A1, suppose that there are M_w number of water molecules, M_L number of chains of the long-chain network and M_S number of chains of the short-chain network in the lattice. Let n_L and n_S denote the number of monomers on each chain of the long-chain and short-chain networks, respectively. The Helmholtz free energy F^m can be expressed as (Flory, 1953)

$$F^m = kT\left[M_w log\phi_w + \sum_{i=L,\ S} M_i log\phi_i + M_w \sum_{i=L,\ S} \chi_i \phi_i\right], \tag{A1}$$

where ϕ_w is the volume fraction of water in the DN gel (represented by the lattice model) and ϕ_i the volume of the polymer network i ($i = L$ and $i = S$ represent the long-chain network and short-chain network, respectively). χ_i is a dimensionless measure of the strength of pairwise interactions between water molecules and monomers of the network i.

As noted in the main text, the dry polymer networks are taken as the reference state to characterize the deformation of the DN gel. Following Flory and Huggins, we assume that the water molecule and monomers of both long-chain and short-chain networks take the same volume ν. Then we can correlate the free energy of mixing W^m with the Helmholtz free energy of mixing F^m by $W^m = F^m/(n_L M_L \nu + n_S M_S \nu)$. Accordingly, W^m takes the form that

$$W^m = \frac{kT}{\nu}\left(\nu C log\phi_w + \frac{M_L}{n_L M_L + n_S M_S} log\phi_L + \frac{M_S}{n_L M_L + n_S M_S} log\phi_S + \nu C\chi_L\phi_L + \nu C\chi_S\phi_S\right), \tag{A2}$$

where $C = \frac{M_w}{n_L M_L \nu + n_S M_S \nu}$ is the number of water molecules per volume of dry polymer networks. We define η_i as the volume fraction of the network i in the dry polymer networks ($\eta_L = \frac{n_L M_L \nu}{n_L M_L \nu + n_S M_S \nu}$, $\eta_S = \frac{n_S M_S \nu}{n_L M_L \nu + n_S M_S \nu}$), such that $\frac{M_L}{n_L M_L + n_S M_S}$ can be simplified as η_L/n_L. Note that $0 < \eta_L < 1$ and n_L commonly takes a large value. Therefore, the term $\frac{M_L}{n_L M_L + n_S M_S} \approx 0$. Similarly, $\frac{M_S}{n_L M_L + n_S M_S}$ also approaches zero. Then Eq. (A2) reduces to

$$W^m = \frac{kT}{\nu}(\nu C log\phi_w + \nu C\chi_L\phi_L + \nu C\chi_S\phi_S). \tag{A3}$$

Note that $C\nu$ is the volume of water molecules in the gel divided by the volume of dry polymer networks and equals to $J - 1$, J is the swelling ratio of the gel, which is defined as the volume of the DN gel divided by the volume of the dry polymer networks. Therefore, the volume fraction of water in the DN gel ϕ_w is equal to $\frac{J-1}{J}$, and the volume fraction of the long-chain and short-chain networks is $\phi_L = \eta_L \frac{1}{J}$ and $\phi_S = \eta_S \frac{1}{J}$, respectively. Eq. (A3) can be rewritten as

$$W^m = \frac{kT}{\nu}\left[(J-1) log\frac{J-1}{J} + \sum_{i=L,\ S} \eta_i \chi_i \frac{J-1}{J}\right]. \tag{A4}$$

Eq. (A4), also listed as Eq. (3) in the main text, gives the free energy of mixing W^m for DN gels.

Appendix B. The calculation of the equilibrium swelling ratio J_0 for DN gels

The initial swelling ratio of the DN gel, i.e., J_0 of the gel in the free-swelling state before any mechanical load is applied, can be obtained by setting $s_1 = s_2 = s_3 = 0$ and $\lambda_1 = \lambda_2 = \lambda_3 = \sqrt[3]{J_0} = \lambda_0$ in Eqs. (11a) and (11b) in the main text, that is,

$$\left(\frac{\eta_S^{\frac{1}{3}}\beta_S}{3\sqrt{n_{S0}}\Lambda_S} exp\left[-\frac{1}{2}p\left(\Lambda_S^{max} - \eta_S^{-\frac{1}{3}}\right)\right] + \frac{\eta_L^{\frac{1}{3}}\beta_L}{3\sqrt{n_L}\Lambda_L}\right)\lambda_0 + \left[log\left(1 - \frac{1}{J}\right) + \frac{1}{J} + \frac{\chi_S\eta_S + \chi_L\eta_L}{J^2}\right]\frac{J}{\lambda_0} = 0. \tag{B1}$$

From Eq. (B1), the initial swelling ratio of the DN gel can be obtained. For instance, in the main text, the DN gel investigated has $n_{S0} = 50$ and $n_L = 2000$, and the corresponding initial swelling ratio of the DN gel can be calculated by solving Eq. (B1), which gives $J_0 = 18.05$, as shown in Fig. 3(b) of the main text.

Appendix C. Threshold for delayed necking of stretched DN gels

The threshold for delayed instability is strongly affected by the material properties of the DN gel, for example, n_L, which characterizes the chain length of long-chain networks. We find that for $n_L > 1697$, the threshold for delayed necking instability is determined by the peak of the long-term equilibrium *s-J* curve; for $n_L < 1697$, the threshold for delayed necking instability is given by the *transition swelling ratio*. Details of the analysis are provided below.

(i) For $n_L > 1697$, we take $n_L = 2000$, the numerical case discussed in the main text, as an example. Note that values of other model parameters adopted in this section are kept the same as those used in the main text. In this case, the peak value of the long-term equilibrium *s-J* curve is $\frac{s_V}{kT} = 6.6 \times 10^{-3}$ [Fig. C1(a)]. If the applied stress $\frac{s_V}{kT}$ is slightly lower than the peak value of the *s-J* curve, the gel swells, ending up with a swelling ratio close to $J = 35.87$. Note that the peak value of the instantaneous *s-λ* curve corresponding to $J = 35.87$ is higher than the applied stress level [Fig. C1(b)], thus necking cannot occur. In contrast, consider another circumstance where the applied stress is equal to 6.6×10^{-3}, the DN gel can swell from the initial swelling ratio $J =$ 18.05 to 94.67 [Fig. C1(a)]. At the moment when the swelling ratio reaches $J = 43.65$, the peak value of the instantaneous *s-λ* curve drops to the applied stress of $\frac{s_V}{kT} = 6.6 \times 10^{-3}$ [Fig. C1(b)], thereby triggering the necking instability after a delay in time. As discussed above, delayed necking occurs at an applied stress equal to 6.6×10^{-3} but is prohibited for applied stresses less than 6.6×10^{-3}. That is, in this case, the threshold for delayed necking instability is 6.6×10^{-3}, the peak value of the long-term equilibrium *s-J* curve.

(ii) For $n_L \leq 1697$, we take $n_L = 1000$ as an example. Distinct from the case with $n_L = 2000$ shown in Fig. C1(a), the equilibrium *s-J* curve for $n_L = 1000$ is monotonic and has no peak [Fig. C2(a)], such that the threshold for delayed instability cannot be directly determined by the equilibrium *s-J* curve. In Fig. C2 (b), we find that the instantaneous stress-stretch curve has a local peak when swelling ratio $J \leq 23.93$, while the curve becomes monotonic when *J* surpasses23.93, indicating that the DN gel with $J > 23.93$ is not susceptible to necking instability. We define the swelling ratio $J = 23.93$, which marks the disappearance of the local peak of the instantaneous *s-λ* curve, as the *transition swelling ratio*. Herein, the peak value of the instantaneous *s-λ* curve corresponding to the transition swelling ratio $J = 23.93$ is 11×10^{-3} [Fig. C2(a)]. When a stress slightly lower than 11×10^{-3} is applied to the DN gel, the equilibrium *s-J* curve demonstrates that the gel can swell from $J = 16.3$ to 60.8. The gel does not develop necking, because the applied stress is lower than peak values of instantaneous *s-λ* curves with $J < 23.93$ and the gel becomes immune from necking instability when *J* surpasses 23.93. However, when a stress equal to 11×10^{-3} is exerted, the peak value of the instantaneous curve drops to the applied stress level when *J* reaches 23.93, thereby leading to delayed necking instability. That is, the threshold for delayed necking instability for $n_L = 1000$ is 11×10^{-3} – the peak value of instantaneous *s-λ* curve corresponding to the transition swelling ratio.

Reference

Bogen, D.K., McMahon, T.A., 1979. Do cardiac aneurysms blow out. Biophys. J. 27, 301–316.
Cai, S., Chen, D., Suo, Z., Hayward, R.C., 2012. Creasing instability of elastomer films. Soft Matter 8, 1301–1304.
Chater, E., Hutchinson, J.W.J.J.o.A.M., 1984. On the propagation of bulges and buckles. 51, 2609-2615.
Chen, D., Cai, S., Suo, Z., Hayward, R.C., 2012. Surface energy as a barrier to creasing of elastomer films: an elastic analogy to classical nucleation. Phys. Rev. Lett. 109.
Chen, Y., Jin, L., 2020. Snapping-back buckling of wide hyperelastic columns. Extreme Mech. Lett. 34.
Cheng, J., Jia, Z., Guo, H., Nie, Z., Li, T., 2019. Delayed burst of a gel balloon. J. Mech. Phys. Solids 124, 143–158.
Flory, P.J., 1953. In principles of polymer chemistry. Principles of Polymer Chemistry.
Flory, P.J., Rehner, J., 1943. Statistical mechanics of cross-linked polymer networks I Rubberlike elasticity. J. Chem. Phys. 11, 512–520.
Fu, Y., Lu, H., Nian, G., Wang, P., Lin, N., Hu, X., Zhou, H., Yu, H., Qu, S., Yang, W., 2020. Size-dependent inertial cavitation of soft materials. J. Mech. Phys. Solids 137.
Fu, Y.B., Liu, J.L., Francisco, G.S., 2016. Localized bulging in an inflated cylindrical tube of arbitrary thickness - the effect of bending stiffness. J. Mech. Phys. Solids 90, 45–60.
Han, Z., Wang, P., Mao, G., Yin, T., Zhong, D., Yiming, B., Hu, X., Jia, Z., Nian, G., Qu, S., Yang, W., 2020. Dual pH-responsive hydrogel actuator for lipophilic drug delivery. ACS Appl. Mater. Interfaces.
Hong, W., Liu, Z., Suo, Z., 2009. Inhomogeneous swelling of a gel in equilibrium with a solvent and mechanical load. Int. J. Solids Struct. 46, 3282–3289.
Hong, W., Zhao, X., Zhou, J., Suo, Z., 2008. A theory of coupled diffusion and large deformation in polymeric gels. J. Mech. Phys. Solids 56, 1779–1793.
Huang, R., 2005. Kinetic wrinkling of an elastic film on a viscoelastic substrate. J. Mech. Phys. Solids 53, 63–89.
Jawed, M.K., Khouri, N.K., Da, F., Grinspun, E., Reis, P.M., 2015. Propulsion and instability of a flexible helical rod rotating in a viscous fluid. Phys. Rev. Lett. 115.
Jin, L., Suo, Z., 2015. Smoothening creases on surfaces of strain-stiffening materials. J. Mech. Phys. Solids 74, 68–79.
Li, B., Cao, Y.-P., Feng, X.-Q., Gao, H., 2011. Surface wrinkling of mucosa induced by volumetric growth: theory, simulation and experiment. J. Mech. Phys. Solids 59, 758–774.
Li, J., Mooney, D.J., 2016. Designing hydrogels for controlled drug delivery. Nat. Rev. Mater. 1.
Liu, Q., Ouchi, T., Jin, L., Hayward, R., Suo, Z., 2019. Elastocapillary crease. Phys. Rev. Lett. 122.
Ma, J., Jia, Z., Qu, S., 2020. A constitutive model for binary-solvent gels. J. Appl. Mech. 87.
Mullin, T., Deschanel, S., Bertoldi, K., Boyce, M.C., 2007. Pattern transformation triggered by deformation. Phys. Rev. Lett. 99.
Na, Y.H., Tanaka, Y., Kawauchi, Y., Furukawa, H., Sumiyoshi, T., Gong, J.P., Osada, Y., 2006. Necking phenomenon of double-network gels. Macromolecules 39, 4641–4645.
Overvelde, J.T.B., Kloek, T., D'Haen, J.J.A., Bertoldi, K., 2015. Amplifying the response of soft actuators by harnessing snap-through instabilities. Proc. Nat. Acad. Sci. U.S.A. 112, 10863–10868.

Rafsanjani, A., Bertoldi, K., 2017. Buckling-induced kirigami. Phys. Rev. Lett. 118.
Tang, J., Li, J., Vlassak, J.J., Suo, Z., 2017. Fatigue fracture of hydrogels. Extreme Mechanics Letters 10, 24–31.
Treloar, L.R.G., Riding, G., 1979. Non-gaussian theory for rubber in biaxial strain .1. Mechanical-properties. Proc. R. Soc. Lond. Ser. a-Math. Phys. Eng. Sci. 369, 261–280.
Wang, Q., Zhang, L., Zhao, X., 2011. Creasing to cratering instability in polymers under ultrahigh electric fields. Phys. Rev. Lett. 106.
Wang, X., Hong, W., 2012. Delayed fracture in gels. Soft Matter 8, 8171–8178.
Yang, H., Ji, M., Yang, M., Shi, M., Pan, Y., Zhou, Y., Qi, H.J., Suo, Z., Tang, J., 2021. Fabricating hydrogels to mimic biological tissues of complex shapes and high fatigue resistance. Matter 4, 1935–1946.
Ye, Y., Liu, Y., Fu, Y., 2020. Weakly nonlinear analysis of localized bulging of an inflated hyperelastic tube of arbitrary wall thickness. J. Mech. Phys. Solids 135.
Yin, J., Cao, Z., Li, C., Sheinman, I., Chen, X., 2008. Stress-driven buckling patterns in spheroidal core/shell structures. Proc. Nat. Acad. Sci. U.S.A. 105, 19132–19135.
Yuk, H., Varela, C.E., Nabzdyk, C.S., Mao, X., Padera, R.F., Roche, E.T., Zhao, X., 2019. Dry double-sided tape for adhesion of wet tissues and devices. Nature 575, 169-+.
Zang, J., Zhao, X., Cao, Y., Hutchinson, J.W., 2012. Localized ridge wrinkling of stiff films on compliant substrates. J. Mech. Phys. Solids 60, 1265–1279.
Zhao, X., 2012. A theory for large deformation and damage of interpenetrating polymer networks. J. Mech. Phys. Solids 60, 319–332.
Zheng, Y., Lai, Y., Hu, Y., Cai, S., 2019. Rayleigh–Taylor instability in a confined elastic soft cylinder. J. Mech. Phys. Solids 131, 221–229.